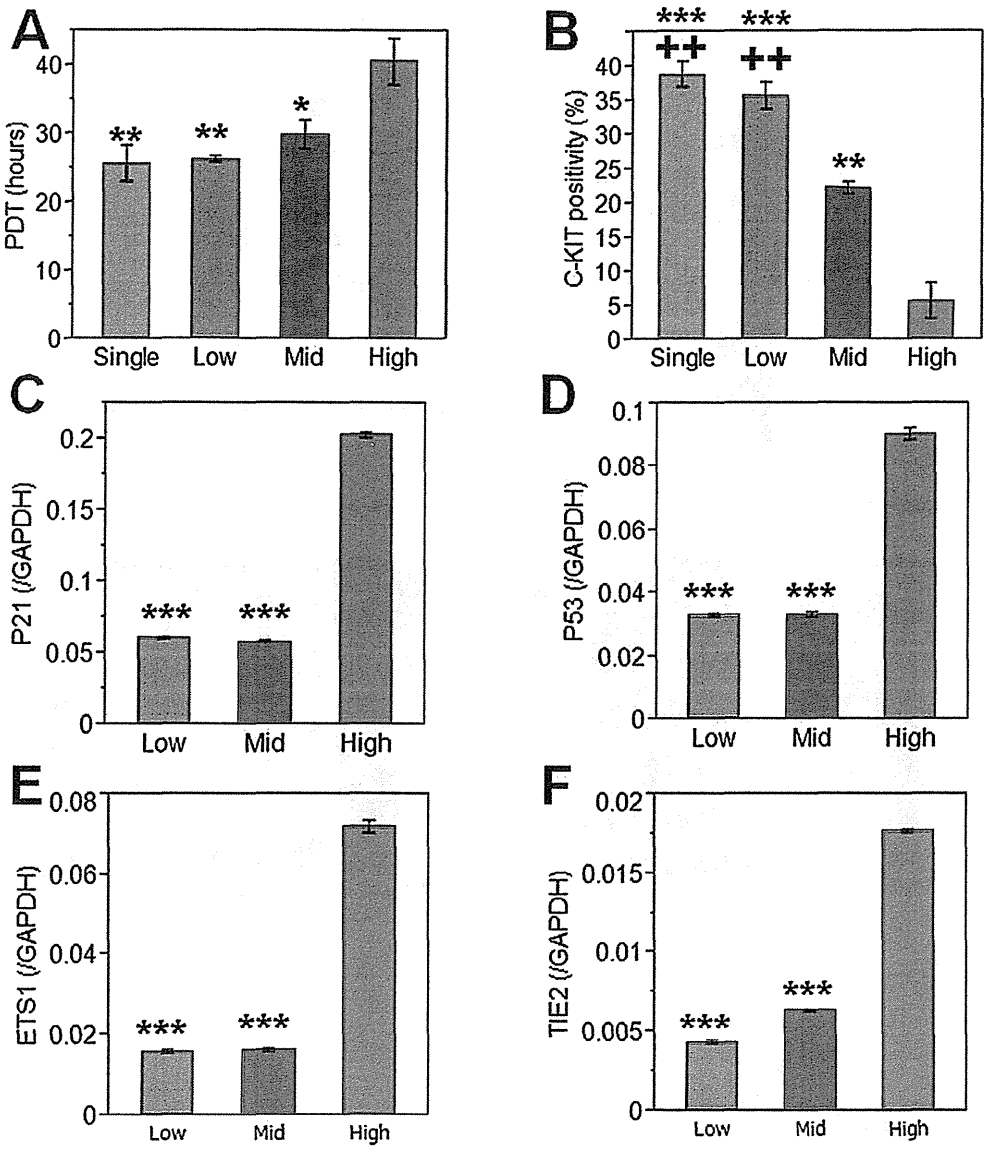

Figure 1. Population doubling time (PDT) and C-KIT positivity in cardiac stem cells. (**A**) PDT was averaged for 3 passages. (**B**) C-KIT positivity was assessed by FACS and averaged for 3 passages. (**C–F**) qPCR analysis. The values are the average for triplicate in a representative experiment. *P<0.05, **P<0.01, ***P<0.0001 vs. "High" group. ++P<0.01 vs. "Mid" group.

Statistical Analysis

All data represent the mean±SEM. Statistical analyses were performed using software (JMP9, SAS Institute Japan, Tokyo, Japan or Prism 5, GraphPad Software, La Jolla, CA, USA). For multiple comparisons, ANOVA with Tukey's HSD post-hoc test was used. For the qPCR analysis of C-KIT, interleukin (IL)-8, and VEGF (Vascular endothelial growth factor) A, the raw data (normalized by GAPDH) of the "High" or "High+GSI" group were normalized to the data of the "Low" group from the same patient, because samples from 3 different patients were used for this experiment, and 1-sample t-test (vs. Low group) or unpaired t-test (High vs. High+GSI group) was used. For echocardiography, the delta values (the difference between before and 3 weeks after the transplantation) were used. If the P-value was <0.05, the difference was considered significant.

Results

Plating Density-Dependent Proliferation Activity and Purity of CSCs

Based on previous reports, we hypothesized that the plating density would affect the proliferation activity and purity of CSCs. We expected that higher plating density would increase Notch signaling, induce differentiation and therefore decrease the proliferation activity and purity of CSCs. To examine this, we isolated CSCs from samples (eg, 5.6×10^5 cells/g muscle at P1). After several passages of culture, we purified C-KIT pos-

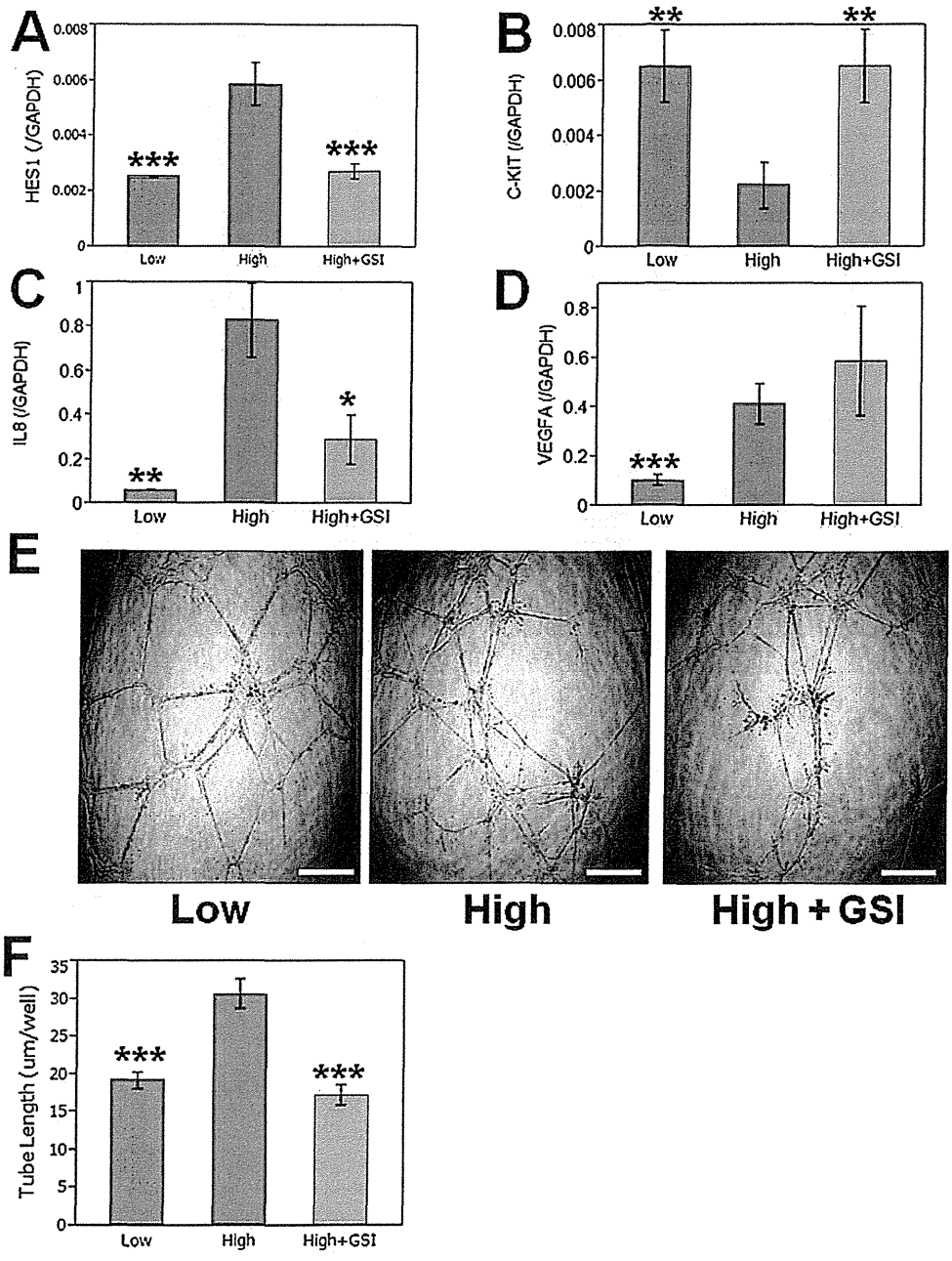

Figure 2. Vascular endothelial cell (EC)differentiation of cardiac stem cells resulting from high-density culture through Notch signaling activation. (**A–D**) qPCR analysis was performed after 3 passages under each plating density condition for the target gene of Notch signaling (*HES1*), C-KIT, and EC-related genes (IL-8 and VEGFA). (**E**) Representative morphologies of tube formation assay are shown. Original magnification, ×20. Scale bars=500 μm. (**F**) Quantitative analysis of the tube formation assay. The total length of tubes per well was measured. The results from 12–14 wells per group were analyzed. *P<0.05, **P<0.01, ***P<0.0001 vs. "High" group.

itive cells by FACS (93.0±0.3%; mean±SEM) and plated at different densities (cells/cm^2): 86 (Single), 340 (Low), 1,400 (Mid), or 5,500 (High).

The proliferation activity of CSCs in relation to plating density was assessed by population doubling time (PDT), which was measured at each passage until the 3rd passage and then averaged (**Figure 1A**). The Single, Low and Mid groups showed a significantly shorter PDT than the High group. Purity of CSCs in relation to plating density was assessed by C-KIT positivity, which was measured at each passage until the 3rd passage and then averaged (**Figure 1B**). The Single and Low groups showed significantly greater C-KIT positivity than

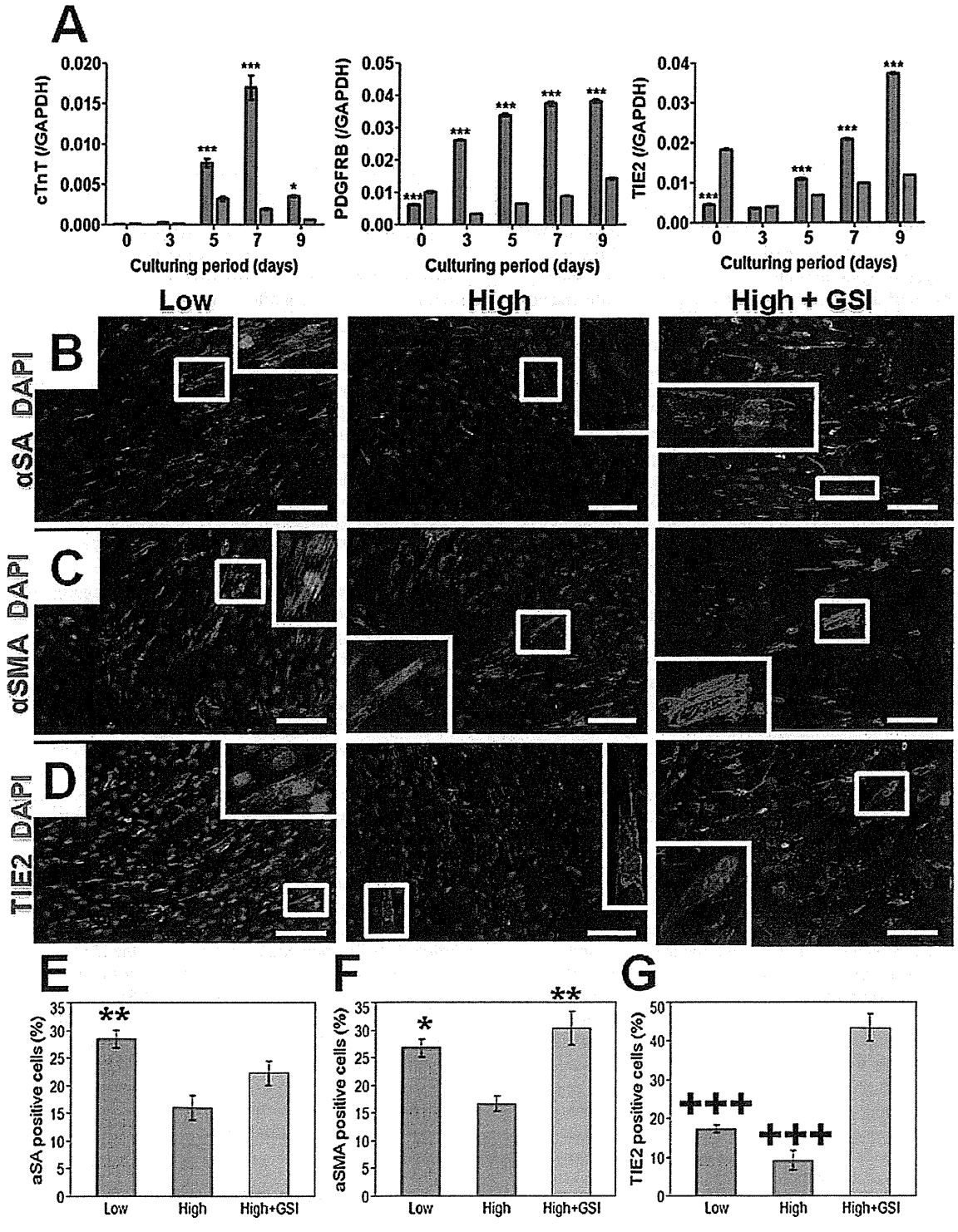

Figure 3. Differentiation potentials of cardiac stem cells (CSC) in vitro. (**A**) CSCs cultured at a low (blue) or high (red) plating density were incubated with dexamethasone for 9 days. The expression levels of cardiomyocyte (cTnT), smooth muscle cell (PDGFRB), and endothelial cell (TIE2) markers were analyzed by qPCR during the culture period. (**B–D**) Immunostaining for differentiated cells on day 7. Scale bars=100 μm. (**E–G**) Quantitative analysis of the immunostaining. The results from 11–20 fields per group were examined. *P<0.05, **P<0.01 vs. "High" group. $^{+++}$P<0.0001 vs. "High+GSI" group.

the Mid and High groups, and the Mid group showed significantly greater C-KIT positivity than the High group. These findings suggested that lower plating cell densities might contribute to preservation of the proliferation activity and purity of CSCs in vitro.

Plating Density-Dependent Transcriptional Profiles of CSCs

Cellular function of CSCs in relation to the plating cell-density and Notch signaling was further assessed by qPCR for cell-cycle regulating genes (P21 and P53), EC markers (ETS1, TIE2, IL8, and VEGFA), Notch-signaling target gene (*HES1*)[23] and C-KIT. Expression of these genes in CSCs was analyzed in the Low, Mid and High groups. In addition, GSI, which is a known Notch signal inhibitor,[16,17,24,25] was added to the culture medium of the High group to investigate the influence of Notch signaling on the gene expression.

The Low and Mid groups showed significantly lower levels of expression of P21, P53, ETS1, and TIE2, compared with the High group (**Figures 1C–F**). In addition, the Low group showed lower expressions of HES1, IL8 and VEGFA than the High group, and C-KIT expression was significantly greater in the Low group than in the High group (**Figures 2A–D**). Of note, the addition of GSI in the High group diminished the expression of HES1 and IL-8, but not of VEGFA. In addition, C-KIT expression in the High group was restored to that of the Low group by GSI treatment (**Figure 2B**). These findings suggested that higher plating densities might induce endothelial differentiation followed by termination of cell cycles, which slows PDT and diminishes the level of expression of C-KIT through Notch signal activation.

Plating density-dependent EC differentiation of CSCs in relation to Notch signaling was further assessed by the tube formation assay on Matrigel in vitro. Consistent with EC marker expression, the High group generated longer tubes than the Low group. Notably, GSI treatment diminished the tube formation activity in the High group to the level of the Low group, indicating active involvement of Notch signaling in the plating density-dependent EC differentiation of CSCs in vitro (**Figures 2E–F**).

Retained Multipotency in CSCs Under Low-Density Culture

Because we confirmed that a higher plating density might induce EC differentiation of CSCs, we next examined the multipotency of CSCs in relation to the plating density by inducing differentiation in vitro. We expected CSCs at a lower plating density to maintain multipotency, and conversely, lose multipotency at a higher plating density. CSCs that were cultured in Low and High conditions were replated with dexamethasone and incubated for 9 days.[3,26,27] Expressions of cTnT (cardiomyocyte marker), PDGFRB (SMC marker), and TIE2 in each group were serially assessed by qPCR. cTnT, PDGFRB, and TIE2 were all upregulated in Low group over the culture period compared with the High group (**Figure 3A**), suggesting that CSCs cultured at low density may retain greater multipotency than those cultured under High conditions.

The differentiation potential of CSCs was further assessed by immunostaining for αSA (cardiomyocyte marker), αSMA (SMC marker) and TIE2 on day 7 (**Figures 3B–D**). The number of αSA- or αSMA-positive cells was significantly greater in the Low group than in the High group, and the TIE2-positive cell number tended to be greater in the Low group than in the High group (**Figures 3E–G**). Of note, the cells cultured under High conditions with GSI showed a significantly greater positivity for αSMA and TIE2 than those under pure High culture conditions, though GSI treatment did not affect significantly αSA positivity. These findings suggested that the multipotency of CSCs was hampered by higher plating density through Notch signaling-mediated EC differentiation.

Therapeutic Effects of CSCs in a Rat AMI Model

Our in vitro data suggested that CSCs at a lower plating density maintained multipotency. Because multipotency may be required for their therapeutic potential, we next examined this in relation to the plating density and Notch signaling by transplanting CSCs into a rat AMI model.[3] We expected CSCs cultured under Low and High+GSI conditions to have greater therapeutic potential than those under High conditions. CSCs that were prepared in Low, High, or High+GSI culture conditions suspended with PBS or PBS only were injected into the infarct-border zone just after permanent ligation of the LCA. Effects of the CSC-transplantation therapy were assessed by standard TTE.

TTE revealed that all groups consistently showed progressive enlargement of the end-diastolic volume of the LV. However, the Low group showed significantly less progressive enlargement in the end-systolic volume of the LV and significantly less progressive reduction in LV ejection fraction compared with the High group, which showed a similar trend to the PBS-only group (**Figures 4A–C**). Notably, the enlarged LV end-systolic volume and reduced LV ejection fraction in the High group were restored to the levels of the Low group by culturing intact CSCs under High+GSI conditions for 3 passages before transplantation. These findings suggested the reduced therapeutic potential of the High group was mediated by Notch signaling activation during cultivation, which compromised the multipotency of CSCs through EC differentiation.

LV Remodeling and Angiogenesis After CSC Transplantation

Because the therapeutic potential of CSCs is dependent not only on multipotency but also paracrine effects, the latter (LV remodeling and angiogenesis) were further assessed histologically at 3 weeks after transplantation. We expected CSCs cultured under Low and High+GSI conditions to show greater paracrine effects than those under High conditions.

The Low and High+GSI groups had reduced area of scarring and preserved structure of LV compared with the High group, which showed a similar scar size and structure to the PBS-only group, as assessed by Masson's trichrome staining (**Figure 4D**). The percentage of fibrosis in the LV was significantly less in the Low and High+GSI groups compared with the PBS-only and High groups (**Figure 4F**). vWF-positive arterioles and capillaries were more prominent in the infarct-border zone of the Low, High and High+GSI groups compared with the PBS-only group (**Figures 4E,G**). These results indicated that not only direct differentiation potential (multipotency) but also the paracrine effect (antifibrotic effect) of the Low and High+GSI groups might be greater than those of the High group.

Differentiation Potential of CSCs in Vivo

Finally, we examined whether the greater multipotency of the Low and High+GSI groups in vitro reflected greater therapeutic potential in vivo as compared with the High group. The phenotypic fate of the transplanted CSCs, in relation to their plating cell-density and Notch signaling, was assessed in excised rat hearts at 3 weeks after transplantation.

MLC and HNA-double-positive cells were present in the infarct-border zone of the Low and High+GSI groups, but were rarely detected in the High group (**Figure 5A**). Quantitative assessment showed that 60% of the HNA-positive transplanted

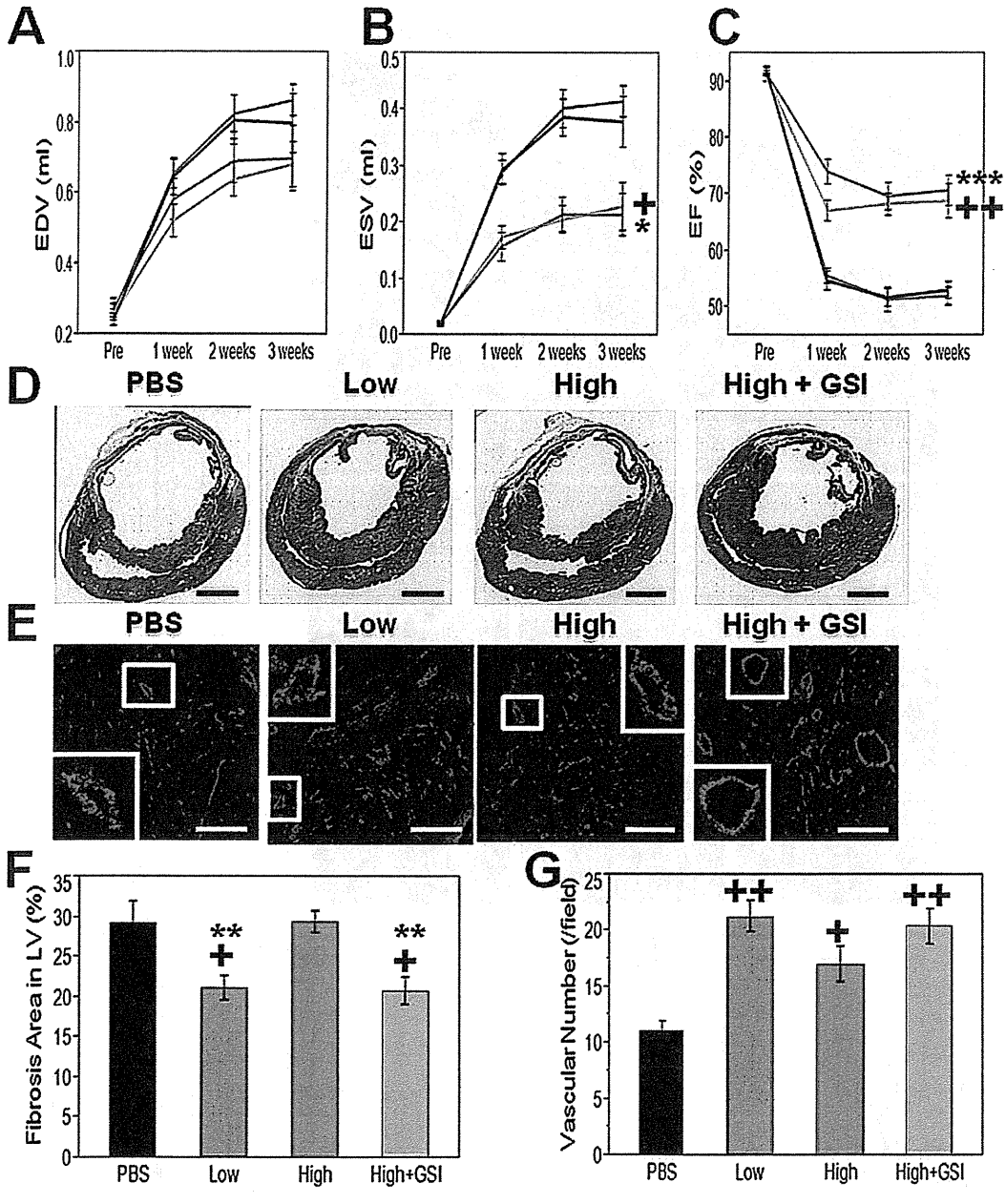

Figure 4. Therapeutic potential of cardiac stem cells in a rat model of acute myocardial infarction. (**A–C**) Echocardiography before (Pre) and after transplantation (1, 2, or 3 weeks). (**A**) End-diastolic volume (EDV, ml), (**B**) end-systolic volume (ESV, ml), (**C**) ejection fraction (EF, %) of rat left ventricle. Black lines indicate PBS treatment, blue lines "Low", red lines "High", and yellow lines "High+GSI" group. The results from 9–11 rats per group were examined. *P<0.05, ***P<0.0001 Low vs. "PBS" and "High" groups. +P<0.05, ++P<0.01 High+GSI vs. "PBS" and "High" groups. (**D–E**) Masson's trichrome staining and immunostaining against vWF. The insets show the enlarged image of the indicated area. Scale bars=2 mm in (**D**) and 200 μm in (**E**). (**F–G**) Quantitative analysis of D and E. (**F**) The results from 9–11 sections at the mid-ventricle level (transplanted site) from 9–11 rats per group were analyzed. (**G**) The results from 54–66 fields from 9–11 rats per group were analyzed. **P<0.01 vs. "High" group. +P<0.05, ++P<0.01 vs. "PBS" group. PBS, phosphate-buffered saline; vWF, von Willebrand factor.

cells in the Low group and 70% in the High plus GSI group were positive for MLC, compared with the High group in which only 20% of the HNA-positive cells were MLC-positive (**Figure 5B**). In addition, the human-derived cardiomyocytes survived at least for 3 weeks after transplantation and resided mainly in the infarct-border zone. These results indicated that the lower plating density with lower Notch signaling maintained the multipotency of CSCs in vitro and their cardiomyogenic differentiation potential in vivo, which resulted in a greater therapeutic potential in the rat model of AMI.

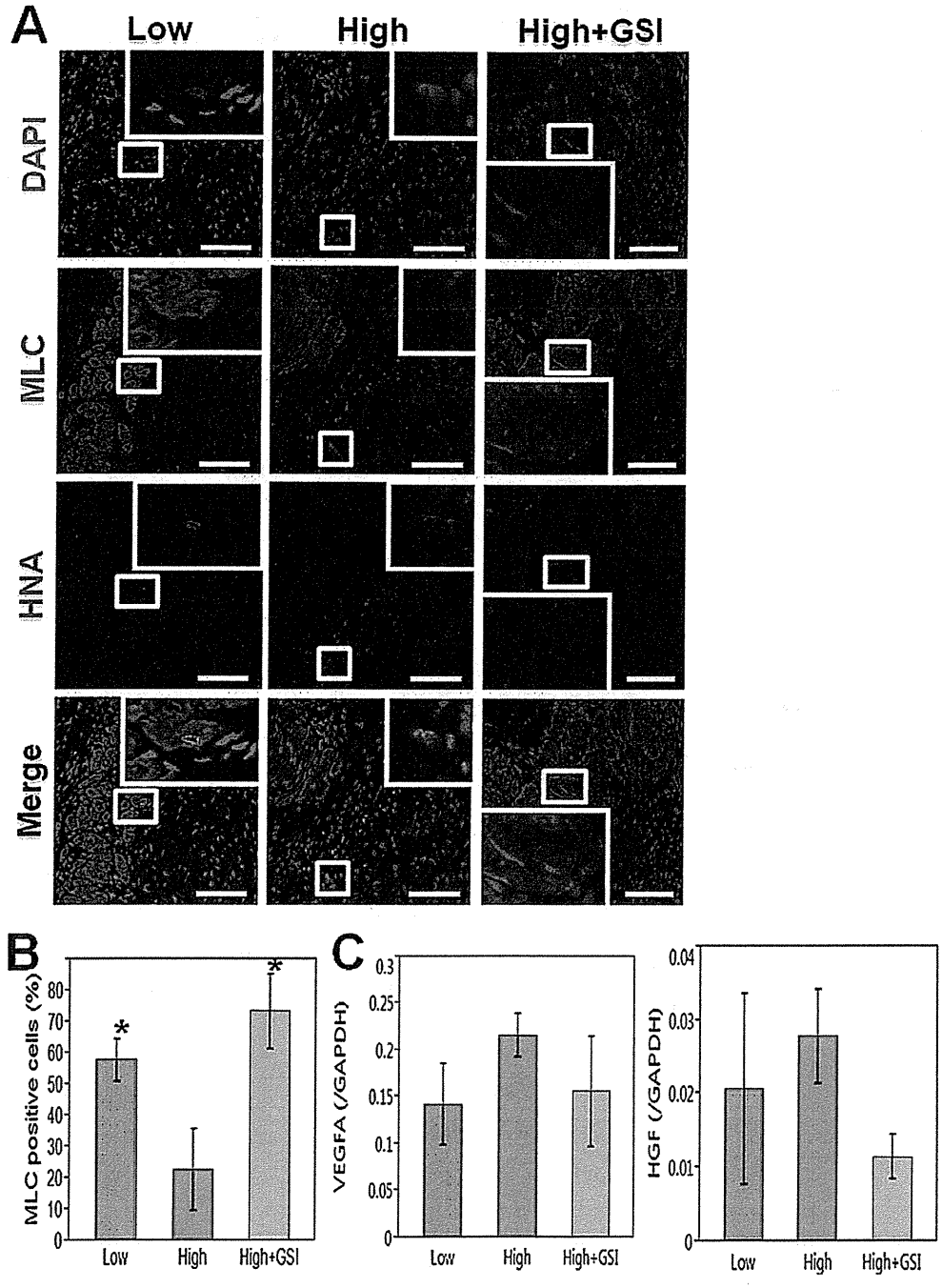

Figure 5. Differentiation potential of cardiac stem cells into cardiomyocytes in vivo. (**A**) Representative images for immunostaining against myosin light chain (MLC, red) and human nuclear antigen (HNA, green). DAPI (blue) was used for nuclear staining. Scale bars=100 μm. (**B**) Quantitative analysis of HNA-positive cells that were MLC-positive in vivo. The results from 10–31 fields per group (from 2–4 rats per group) were analyzed. *P<0.05 vs. "High" group. (**C**) qPCR analysis for VEGFA and HGF. Rat hearts were collected at 2 days after transplantation. GAPDH was used as internal control; 3–4 rats per group were used.

Regarding the paracrine effects, we examined by qPCR some paracrine factors (VEGFA and HGF)[4] at 2 days after transplantation. These experiments showed no significant difference in the expression levels of the paracrine factors among the groups (**Figure 5C**).

Discussion

We discovered that Notch signaling was activated in CSCs under high cell-plating conditions and induced EC differentiation. Notch signaling is implicated as a key regulator of arte-

rial EC differentiation from Flk1-positive endothelial precursors.[28] In addition, VEGF is a known key regulator of EC differentiation from embryonic stem cells.[29] In this study, VEGFA and Notch signaling were both activated in the High group (**Figures 2A,D**). Moreover, the use of GSI clearly dissected the difference in downstream angiogenic gene expressions and in angiogenic potential between the low- and high-density cultures (**Figures 2C,E,F**). Thus, the results from this study lead to the conclusion that Notch signaling is involved in the EC differentiation of CSCs.

C-KIT positivity was markedly reduced during cultivation regardless of the plating cell-density in this study, though previous reports suggested that C-KIT positivity was preserved for several passages until transplantation.[3,7] This contrary finding between the present and the previous studies may be explained by different patient population, sampling/isolation protocols, culture protocols including plating cell-density, and/or different C-KIT detection protocols.[3,7] Although a direct relationship between C-KIT positivity and the therapeutic effects of CSCs remains unclear, plating cell-density was related to C-KIT positivity and therapeutic effects in this study, warranting further studies to investigate the significance of C-KIT expression in this treatment. In addition, the absolute number of C-KIT positive cells increased under low-density conditions compared with the high-density conditions (**Figure S1A**). Thus, low-density conditions might propagate CSCs effectively. In addition, we confirmed that CSCs expressed KDR but not Nkx2.5 (**Figure S3C**). Therefore, the characteristics of CSCs might be similar to those of cardiovascular progenitors.[12,30]

The findings of this study suggested that plating cell-density was a determinant of in vitro fundamental cellular function, including multipotency and the in vivo therapeutic effects of CSCs, and that Notch signal is one of the mechanisms responsible for this plating density-dependent function. CSCs that were cultured under High conditions showed a trend in EC differentiation with loss of SC properties such as multipotency. Although this spontaneous differentiation of CSCs was associated with activation of the Notch signaling pathway, inhibition of Notch signaling using GSI did not totally restore cellular function, including C-KIT positivity and PDT (**Figure S1B**).

One may consider several reasons for this as follows. Firstly, the Notch signal pathway was not totally inhibited by GSI treatment, though the concentration of GSI was carefully prepared by referring to a previous report[16] and doing preliminary experiments (**Figures S1C–E**). Secondly, alternative pathways to Notch signaling are present that may affect cellular properties in the maintenance culture of CSCs.[17,25,31] Finally, Notch signaling in the Low group might be slightly activated during the culture process and thus affect the properties of CSCs.

The magnitude of the therapeutic effects of CSCs in the rat AMI model was dependent upon the plating density in association with Notch signaling in this study. Although inhibition of Notch signaling in the High group did not totally restore cellular functions in vitro (**Figures 2D,3E**), functional and pathological recovery from AMI in the High group was totally restored by inhibition of Notch signaling during the course of cell preparation. This contrary finding may be explained by differences in cellular functions between in vitro and after transplantation into a rat AMI model. The cells that were transplanted into the heart were influenced by a variety of factors, such as needle injection-related mechanical damage, ischemia, inflammation or factors released from the native cardiac tissue.[32,33] These complex pathways in this treatment may yield different results for in vitro and in vivo experiments.

Regarding the therapeutic potential of CSCs, not only the cardiomyogenic potential but also differentiation potential into other lineages or just the proliferative activity of the cells might be considered. However, only a few CSC-derived vWF-positive ECs were detected (**Figure S2A**). For the SMCs, a significant difference in the percentage of αSMA-positive cells was observed between not only the Low and High groups but also the Low and High+GSI groups (**Figure S2B**). In addition, the difference in proliferative activity in vitro might not explain the difference in therapeutic potential between the Low and High groups because the High+GSI group did not recover PDT (**Figure S1B**). Therefore, we conclude that the cardiomyogenic differentiation potential might be the main difference between the Low and High groups in terms of therapeutic potential, which was affected by Notch signaling.

In addition, we also examined the paracrine effect of transplanted CSCs and observed no significant difference in the VEGFA or HGF (**Figure 5C**) (and IGF1; **Figure S2C**) expression levels[4] among the groups (Low vs. High vs. High+GSI) at 2 days after transplantation. This was contrary to results shown in **Figures 4D,F**, which indicated that the antifibrotic effect (possibly by paracrine mechanisms) was hampered by culturing CSCs at a higher plating density. Therefore, other unknown factor(s) might be present and the "High" culture condition might hamper the expression of such protein(s) after transplantation.

This study is limited by the use of primary CSCs from mainly 1 individual patient who had idiopathic cardiomyopathy (except qPCR for C-KIT, IL-8, and VEGFA, in which 3 different patients' samples were used; **Figures 2B–D**), though a consistent fundamental difference in the cellular behavior of primary CSCs cultured with different plating densities was confirmed (PDTs with 4 different patient samples and C-KIT positivity with another patient sample; **Figures S3A,B**).

Regarding CSC preparation in the clinical scenario, the use of Notch signaling inhibitor in the culture process may be useful in enhancing the therapeutic potential of CSCs.[34] In addition, regarding the duration of the existence and localization of the transplanted cells, human-derived cardiomyocytes survived at least for 3 weeks after transplantation and resided mainly in the infarct-border zone. In this study, CSCs of human origin were transplanted into athymic nude rats. This xenotransplantation model has been used in a number of studies, which have rarely reported significant immunological reactions.[22,35] In fact, the transplanted cells in this study were not histologically involved in inflammatory reactions such as accumulation of inflammatory cells (data not shown). Thus, immune rejection in this model is minimal and does not affect the results. In addition, CSCs will be transplanted in an autologous manner in the clinical situation.[6] Therefore, the immunological reactions of this treatment may be negligible.

In conclusion, cellular properties and therapeutic potential of CSCs are affected by cell-plating density through activation of Notch signaling. Therapeutic effects of CSC-transplantation therapy for heart disease may be enhanced by reducing Notch signaling in CSCs.

Acknowledgments

This study was financially supported by a Health Labor Sciences Research Grant from the Japanese Ministry of Health, Labor and Welfare. T.M. was supported by a Grant-in-Aid from the Japan Society for the Promotion of Science Fellows. We thank Professor Piero Anversa (Brigham and Women's Hospital, Boston, USA) and his laboratory members for technical advice. We also thank Ms Masako Yokoyama for technical instruction, Ms Atsuko Shimai and Ms Yuka Takaoka (all from Osaka University), and Ms

Noriko Kakuta (Institute of Biomedical Research and Innovation) for assistance with the manuscript.

References

1. Roger VL, Go AS, Lloyd-Jones DM, Adams RJ, Berry JD, Brown TM, et al. Heart disease and stroke statistics: 2011 update. A report from the American Heart Association. *Circulation* 2011; **123:** e18–e209, doi:10.1161/CIR.0b013e3182009701.
2. Yamauchi T, Miyata H, Sakaguchi T, Miyagawa S, Yoshikawa Y, Takeda K, et al. Coronary artery bypass grafting in hemodialysis-dependent patients: Analysis of Japan Adult Cardiovascular Surgery Database. *Circ J* 2012; **76:** 1115–1120.
3. Bearzi C, Rota M, Hosoda T, Tillmanns J, Nascimbene A, De Angelis A, et al. Human cardiac stem cells. *Proc Natl Acad Sci USA* 2007; **104:** 14068–14073.
4. Chimenti I, Smith RR, Li TS, Gerstenblith G, Messina E, Giacomello A, et al. Relative roles of direct regeneration versus paracrine effects of human cardiosphere-derived cells transplanted into infarcted mice. *Circ Res* 2010; **106:** 971–980.
5. Choi SH, Jung SY, Kwon SM, Baek SH. Perspectives on stem cell therapy for cardiac regeneration: Advances and challenges. *Circ J* 2012; **76:** 1307–1312.
6. Bolli R, Chugh AR, D'Amario D, Loughran JH, Stoddard MF, Ikram S, et al. Cardiac stem cells in patients with ischaemic cardiomyopathy (SCIPIO): Initial results of a randomised phase 1 trial. *Lancet* 2011; **378:** 1847–1857.
7. D'Amario D, Fiorini C, Campbell PM, Goichberg P, Sanada F, Zheng H, et al. Functionally competent cardiac stem cells can be isolated from endomyocardial biopsies of patients with advanced cardiomyopathies. *Circ Res* 2011; **108:** 857–861.
8. Bartosh TJ, Wang Z, Rosales AA, Dimitrijevich SD, Roque RS. 3D-model of adult cardiac stem cells promotes cardiac differentiation and resistance to oxidative stress. *J Cell Biochem* 2008; **105:** 612–623.
9. Tang YL, Zhu W, Cheng M, Chen L, Zhang J, Sun T, et al. Hypoxic preconditioning enhances the benefit of cardiac progenitor cell therapy for treatment of myocardial infarction by inducing CXCR4 expression. *Circ Res* 2009; **104:** 1209–1216.
10. Messina E, De Angelis L, Frati G, Morrone S, Chimenti S, Fiordaliso F, et al. Isolation and expansion of adult cardiac stem cells from human and murine heart. *Circ Res* 2004; **95:** 911–921.
11. Tomita Y, Matsumura K, Wakamatsu Y, Matsuzaki Y, Shibuya I, Kawaguchi H, et al. Cardiac neural crest cells contribute to the dormant multipotent stem cell in the mammalian heart. *J Cell Biol* 2005; **170:** 1135–1146.
12. Yang L, Soonpaa MH, Adler ED, Roepke TK, Kattman SJ, Kennedy M, et al. Human cardiovascular progenitor cells develop from a KDR+ embryonic-stem-cell-derived population. *Nature* 2008; **453:** 524–528.
13. Bu L, Jiang X, Martin-Puig S, Caron L, Zhu S, Shao Y, et al. Human ISL1 heart progenitors generate diverse multipotent cardiovascular cell lineages. *Nature* 2009; **460:** 113–117.
14. Sekiya I, Larson BL, Smith JR, Pochampally R, Cui JG, Prockop DJ. Expansion of human adult stem cells from bone marrow stroma: Conditions that maximize the yields of early progenitors and evaluate their quality. *Stem Cells* 2002; **20:** 530–541.
15. Yanagisawa M, Mukai A, Shiomi K, Song SY, Hashimoto N. Community effect triggers terminal differentiation of myogenic cells derived from muscle satellite cells by quenching Smad signaling. *Exp Cell Res* 2011; **317:** 221–233.
16. Boni A, Urbanek K, Nascimbene A, Hosoda T, Zheng H, Delucchi F, et al. Notch1 regulates the fate of cardiac progenitor cells. *Proc Natl Acad Sci USA* 2008; **105:** 15529–15534.
17. Chen VC, Stull R, Joo D, Cheng X, Keller G. Notch signaling re-specifies the hemangioblast to a cardiac fate. *Nat Biotechnol* 2008; **26:** 1169–1178.
18. Kwon C, Qian L, Cheng P, Nigam V, Arnold J, Srivastava D. A regulatory pathway involving Notch1/beta-catenin/Isl1 determines cardiac progenitor cell fate. *Nat Cell Biol* 2009; **11:** 951–957.
19. Obi S, Masuda H, Shizuno T, Sato A, Yamamoto K, Ando J, et al. Fluid shear stress induces differentiation of circulating phenotype endothelial progenitor cells. *Am J Physiol Cell Physiol* 2012; **303:** C595–C606.
20. Gomes SA, Rangel EB, Premer C, Dulce RA, Cao Y, Florea V, et al. S-nitrosoglutathione reductase (GSNOR) enhances vasculogenesis by mesenchymal stem cells. *Proc Natl Acad Sci USA* 2013; **110:** 2834–2839.
21. Imanishi Y, Saito A, Komoda H, Kitagawa-Sakakida S, Miyagawa S, Kondoh H, et al. Allogenic mesenchymal stem cell transplantation has a therapeutic effect in acute myocardial infarction in rats. *J Mol Cell Cardiol* 2008; **44:** 662–671.
22. Iwasaki H, Kawamoto A, Ishikawa M, Oyamada A, Nakamori S, Nishimura H, et al. Dose-dependent contribution of CD34-positive cell transplantation to concurrent vasculogenesis and cardiomyogenesis for functional regenerative recovery after myocardial infarction. *Circulation* 2006; **113:** 1311–1325.
23. Bray SJ. Notch signalling: A simple pathway becomes complex. *Nat Rev Mol Cell Biol* 2006; **7:** 678–689.
24. Urbanek K, Cabral-da-Silva MC, Ide-Iwata N, Maestroni S, Delucchi F, Zheng H, et al. Inhibition of notch1-dependent cardiomyogenesis leads to a dilated myopathy in the neonatal heart. *Circ Res* 2010; **107:** 429–441.
25. Zakharova L, Nural-Guvener H, Gaballa MA. Cardiac explant-derived cells are regulated by Notch-modulated mesenchymal transition. *PLoS One* 2012; **7:** e37800, doi:10.13731/journal.pone.0037800.
26. Beltrami AP, Barlucchi L, Torella D, Baker M, Limana F, Chimenti S, et al. Adult cardiac stem cells are multipotent and support myocardial regeneration. *Cell* 2003; **114:** 763–776.
27. Fischer KM, Cottage CT, Wu W, Din S, Gude NA, Avitabile D, et al. Enhancement of myocardial regeneration through genetic engineering of cardiac progenitor cells expressing Pim-1 kinase. *Circulation* 2009; **120:** 2077–2087.
28. Lanner F, Sohl M, Farnebo F. Functional arterial and venous fate is determined by graded VEGF signaling and notch status during embryonic stem cell differentiation. *Arterioscler Thromb Vasc Biol* 2007; **27:** 487–493.
29. Tan KS, Tamura K, Lai MI, Veerakumarasivam A, Nakanishi Y, Ogawa M, et al. Molecular pathways governing development of vascular endothelial cells from ES/iPS Cells. *Stem Cell Rev* 2013 June 14, doi:10.1007/s12015-013-9450-7 [Epub ahead of print].
30. Bearzi C, Leri A, Lo Monaco F, Rota M, Gonzalez A, Hosoda T, et al. Identification of a coronary vascular progenitor cell in the human heart. *Proc Natl Acad Sci USA* 2009; **106:** 15885–15890.
31. Shahi P, Seethammagari MR, Valdez JM, Xin L, Spencer DM. Wnt and Notch pathways have interrelated opposing roles on prostate progenitor cell proliferation and differentiation. *Stem Cells* 2011; **29:** 678–688.
32. Segers VF, Lee RT. Stem-cell therapy for cardiac disease. *Nature* 2008; **451:** 937–942.
33. Dimmeler S, Burchfield J, Zeiher AM. Cell-based therapy of myocardial infarction. *Arterioscler Thromb Vasc Biol* 2008; **28:** 208–216.
34. Coric V, van Dyck CH, Salloway S, Andreasen N, Brody M, Richter RW, et al. Safety and tolerability of the gamma-secretase inhibitor avagacestat in a Phase 2 study of mild to moderate alzheimer disease. *Arch Neurol* 2012; **69:** 1430–1440.
35. Alshammary S, Fukushima S, Miyagawa S, Matsuda T, Nishi H, Saito A, et al. Impact of cardiac stem cell sheet transplantation on myocardial infarction. *Surg Today* 2013 March 5, doi:10.1007/s00595-013-0528-2 [Epub ahead of print].

Supplementary Files

Supplementary File 1

Figure S1. C-KIT positive cell number, population doubling time (PDT), and qPCR analysis for cardiac stem cells under different plating densities with and without gamma secretase inhibitor (GSI).

Figure S2. Percentages of transplanted cell-derived differentiated cells in vivo and expression levels of human-specific IGF1 after transplantation.

Figure S3. Population dougling time (PDT) from 4 different patient samples, C-KIT positivity of another patient sample with different plating densities, and RT-PCR analysis for CSCs.

Please find supplementary file(s);
http://dx.doi.org/10.1253/circj.CJ-13-0534

ORIGINAL ARTICLE

BNIP3 Plays Crucial Roles in the Differentiation and Maintenance of Epidermal Keratinocytes

Mariko Moriyama[1,2,4], Hiroyuki Moriyama[1,4], Junki Uda[1], Akifumi Matsuyama[2], Masatake Osawa[3] and Takao Hayakawa[1]

Transcriptome analysis of the epidermis of *Hes1*$^{-/-}$ mouse revealed the direct relationship between Hes1 (hairy and enhancer of split-1) and BNIP3 (BCL2 and adenovirus E1B 19-kDa-interacting protein 3), a potent inducer of autophagy. Keratinocyte differentiation is going along with activation of lysosomal enzymes and organelle clearance, expecting the contribution of autophagy in this process. We found that BNIP3 was expressed in the suprabasal layer of the epidermis, where autophagosome formation is normally observed. Forced expression of BNIP3 in human primary epidermal keratinocytes (HPEKs) resulted in autophagy induction and keratinocyte differentiation, whereas knockdown of BNIP3 had the opposite effect. Intriguingly, addition of an autophagy inhibitor significantly suppressed the BNIP3-stimulated differentiation of keratinocytes, suggesting that BNIP3 plays a crucial role in keratinocyte differentiation by inducing autophagy. Furthermore, the number of dead cells increased in the human epidermal equivalent of BNIP3 knockdown keratinocytes, which suggests that BNIP3 is important for maintenance of skin epidermis. Interestingly, although UVB irradiation stimulated BNIP3 expression and cleavage of caspase3, suppression of UVB-induced BNIP3 expression led to further increase in cleaved caspase3 levels. This suggests that BNIP3 has a protective effect against UVB-induced apoptosis in keratinocytes. Overall, our data provide valuable insights into the role of BNIP3 in the differentiation and maintenance of epidermal keratinocytes.

Journal of Investigative Dermatology advance online publication, 6 February 2014; doi:10.1038/jid.2014.11

INTRODUCTION

The skin epidermis is a stratified epithelium. Stratification is a key process of epidermal development. During epidermal development, the single layer of basal cells undergoes asymmetric cell division to stratify, and produce committed suprabasal cells on the basal layer. These suprabasal cells are still immature and sustain several rounds of cell divisions to form fully stratified epithelia. Recent studies have identified numerous molecules involved in epidermal development, although how these molecules coordinate to induce proper stratification of the epidermis remains to be elucidated. Previously, by integrating both loss- and gain-of-function studies of Notch receptors and their downstream target Hes1 (hairy and enhancer of split-1), we demonstrated the multiple roles of Notch signaling in the regulation of suprabasal cells (Moriyama *et al.*, 2008). Notch signaling induces differentiation of suprabasal cells in a Hes1-independent manner, whereas Hes1 is required for maintenance of the immature status of suprabasal cells by preventing premature differentiation. In light of the critical role of Hes1 in the maintenance of spinous cells, exploration of the molecular targets of Hes1 in spinous layer cells may lead to the discovery of the molecules required for differentiation of spinous layer cells to granular layer cells. Because Hes1 is thought to be a transcriptional repressor (Ohtsuka *et al.*, 1999), loss of Hes1 is expected to cause aberrant upregulation of genes that are normally repressed in spinous layer cells. To identify these genes, we previously conducted comparative global transcript analysis using microarrays and found several candidates that may play a crucial role in regulating epidermal development (Moriyama *et al.*, 2008). One of the genes that was highly expressed was *BNIP3* (*BCL2 and adenovirus E1B 19-kDa-interacting protein 3*), an atypical pro-apoptotic BH3-only protein that induces cell death and autophagy (Zhang and Ney, 2009).

The molecular mechanism through which BNIP3 induces cell death is not well understood; however, it has been reported that BNIP3 protein is induced by hypoxia in some tumor cells and that the kinetics of this induction correlate with cell death (Sowter *et al.*, 2001). In contrast,

[1]*Pharmaceutical Research and Technology Institute, Kinki University, Higashi-Osaka, Osaka, Japan;* [2]*Platform for Realization of Regenerative Medicine, Foundation for Biomedical Research and Innovation, Kobe, Hyogo, Japan and* [3]*Division of Regeneration Technology, Gifu University School of Medicine, Gifu, Gifu, Japan*

[4]*These authors contributed equally to this work.*

Correspondence: Mariko Moriyama, Pharmaceutical Research and Technology Institute, Kinki University, Higashi-Osaka, Osaka 577-8502, Japan. E-mail: mariko@phar.kindai.ac.jp

Abbreviations: 3-MA, 3-methyladenine; BNIP3, BCL2 and adenovirus E1B 19-kDa-interacting protein 3; ChIP, chromatin immunoprecipitation; Hes1, hairy and enhancer of split-1; HPEK, human primary epidermal keratinocyte; Q-PCR, quantitative PCR

Received 18 July 2013; revised 10 December 2013; accepted 18 December 2013; accepted article preview online 8 January 2014

BNIP3-induced autophagy has been shown to protect HL-1 myocytes from cell death in an ischemia–reperfusion model (Hamacher-Brady *et al.*, 2007). Induction of autophagy by BNIP3 has a protective effect in some conditions, whereas in others it is associated with autophagic cell death. Recent evidence also suggests that BNIP3, through autophagy, is also required for the differentiation of chondrocytes under hypoxic conditions (Zhao *et al.*, 2012).

Autophagy was initially described based on its ultrastructural features of the double-membraned structures that surrounded the cytoplasm and organelles in cells, known as autophagosomes (Mizushima *et al.*, 2010). To date, only microtubule-associated protein light chain 3 (LC3), a mammalian homolog of yeast Atg8, is known to be expressed in autophagosomes and, therefore, it serves as a widely used marker for autophagosomes (Kabeya *et al.*, 2000; Mizushima *et al.*, 2004). Autophagy is an evolutionarily conserved catabolic program that is activated in response to starvation or changing nutrient conditions. Recently, autophagy was shown to be involved in differentiation of multiple cell types, including erythrocytes, lymphocytes, adipocyte, neuron, and chondrocyte (Srinivas *et al.*, 2009; Mizushima and Levine, 2010).

Epidermal cornification, the process of terminal keratinocyte differentiation, requires programmed cell death in a similar but different pathway from apoptosis (Lippens *et al.*, 2005). Cornification is also accompanied by activation of lysosomal enzymes and organelle clearance. Moreover, some researchers have reported that autophagy may play a role in epidermal differentiation (Haruna *et al.*, 2008; Aymard *et al.*, 2011; Chatterjea *et al.*, 2011). Therefore, it is likely that BNIP3 is involved in cornification through cell death or autophagy.

In this study, transcriptome analysis of *Hes1*$^{-/-}$ mouse epidermis revealed that Hes1 could directly suppress BNIP3 expression in epidermal keratinocytes. We also found that BNIP3 was expressed in the suprabasal layer of the human skin epidermis, where autophagosome formation was observed. BNIP3 was also sufficient to promote cornification through induction of autophagy. Finally, we found that BNIP3 had a protective effect against UVB-induced apoptosis in keratinocytes *in vitro*. Our data thus indicate that BNIP3, an inducer of autophagy, is involved in the terminal differentiation and maintenance of epidermal keratinocytes.

RESULTS

Hes1 directly represses BNIP3 expression in epidermal cells and keratinocytes

We previously performed a microarray analysis with epidermal RNAs isolated from wild-type and *Hes1*$^{-/-}$ mice (Moriyama *et al.*, 2008) and found that BNIP3 was preferentially overexpressed in *Hes1*$^{-/-}$ epidermis. The upregulation of *Bnip3* in the *Hes1*$^{-/-}$ epidermis was confirmed by quantitative PCR (Q-PCR) and immunofluorescent staining (Figure 1a and b). As Hes1 is thought to be a transcriptional repressor (Ishibashi *et al.*, 1994), it might play a repressive role in the regulation of BNIP3 expression. In accordance with this hypothesis, BNIP3 expression in *Hes1*$^{-/-}$ epidermis at embryonic day 15.5 was observed in the suprabasal layers (Figure 1b), where Hes1 has been reported to be expressed in wild-type epidermis at the same age (Blanpain *et al.*, 2006; Moriyama *et al.*, 2008). To confirm whether Hes1 suppresses BNIP3 expression, an adenoviral vector expressing Hes1 was used to infect human primary epidermal keratinocytes (HPEKs) and, subsequently, the expression level of BNIP3 was quantified by Q-PCR and western blot analysis. The BNIP3 protein was detected as multiple bands between 22 and 30 kD as previously reported (Vengellur and LaPres, 2004; Walls *et al.*, 2009; Mellor *et al.*, 2010; Sassone *et al.*, 2010). We found that Hes1 induced a substantial reduction of BNIP3 expression in HPEKs at the mRNA and protein levels (Figure 1c and d), demonstrating that Hes1 is involved in the repression of BNIP3. To determine whether Hes1 directly regulates *BNIP3* expression, we performed chromatin immunoprecipitation (ChIP) assays. We identified at least 5 Hes1 consensus binding sites 1 kb upstream of the transcription initiation site of the human *BNIP3* gene, and subsequent Q-PCR analysis revealed that a DNA fragment located at -247 to -87 was slightly amplified from crosslinked chromatin isolated by Hes1 immunoprecipitation (Figure 1e). We also found an additional site between -212 and $+22$ that was strongly amplified. These data clearly show that Hes1 specifically binds to the promoter region of *BNIP3* and directly suppresses its expression.

BNIP3 is expressed in the granular layer of the epidermis, where autophagosome formation is observed

To determine the BNIP3 expression profile in the epidermis, we performed immunofluorescent staining in human skin epidermal equivalent. BNIP3 was expressed in the granular layer of epidermal equivalent 18 days (Figure 2a and b) or 24 days (Figure 2c and d) after exposure at the air–liquid interface. BNIP3 expression in the granular layer was also observed in the normal human skin epidermis (Figure 2g and h). Recent reports show that BNIP3 is expressed in mitochondria and that it induces autophagy (Quinsay *et al.*, 2010). In addition, some researchers have reported that autophagy may play a role in epidermal differentiation (Haruna *et al.*, 2008; Aymard *et al.*, 2011; Chatterjea *et al.*, 2011). We therefore investigated whether autophagy occurred in the epidermis, especially in the granular layers. To quantitate the level of autophagy, cytosol to membrane translocation of the autophagy marker EGFP-LC3 (Kabeya *et al.*, 2000) was monitored in a human skin equivalent model (Mizushima *et al.*, 2004). When autophagy is active, autophagosomes containing EGFP-LC3 are visible as fluorescent puncta (Kabeya *et al.*, 2000). As expected, EGFP-LC3 puncta were observed in the granular layers of the epidermal equivalent (Figure 2e). Moreover, endogenous LC3 dots were observed in the granular layers of normal human skin epidermis (Figure 2f). These data suggested that BNIP3 might be involved in the induction of autophagy in the granular layer of the epidermis.

BNIP3 is required for terminal differentiation of keratinocyte by induction of autophagy *in vitro*

To investigate the involvement of BNIP3 in the induction of autophagy, we transduced HPEKs stably expressing EGFP-LC3

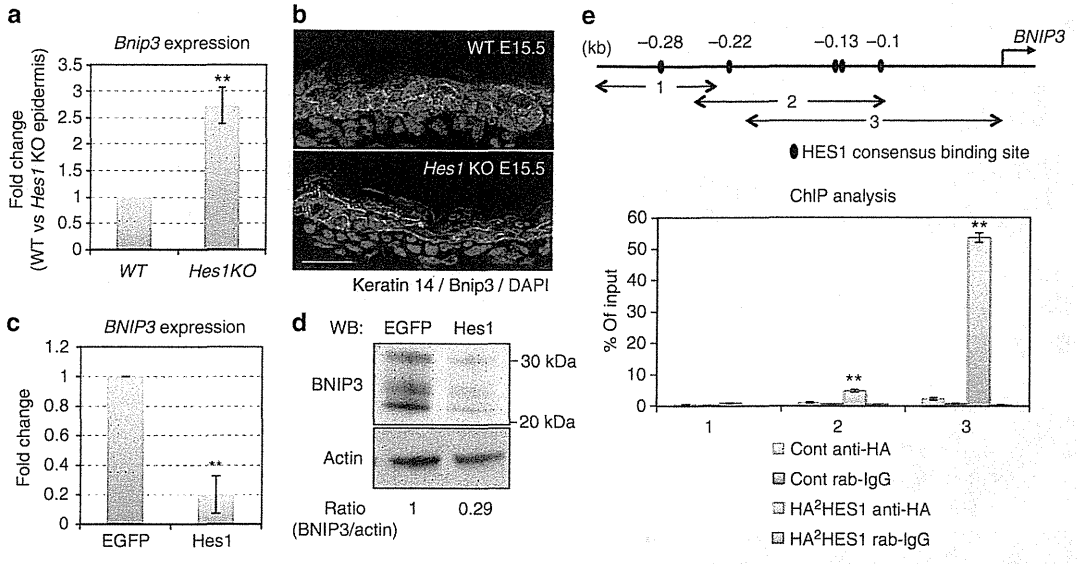

Figure 1. BNIP3 (BCL2 and adenovirus E1B 19-kDa-interacting protein 3) is directly suppressed by HES1(hairy and enhancer of split-1). (**a**) Quantitative PCR (Q-PCR) analysis of *Bnip3* expression in dorsal skin epidermis from either wild-type (WT) or *Hes1* knockout (KO) embryo (embryonic day 14.5 (E14.5)). (**b**) Immunofluorescent analysis of Bnip3 expression in dorsal skin epidermis from either WT or *Hes1* KO embryo (E15.5). Keratin 14 staining is shown in green and Bnip3 staining is shown in red. The blue signals indicate nuclear staining. Scale bars = 20 μm. (**c**) Q-PCR and (**d**) western blot analysis of BNIP3 expression in human primary epidermal keratinocyte (HPEK) cells infected with adenoviruses expressing enhanced green fluorescent protein (EGFP) or Hes1. (**c**) Each expression value was calculated with the ΔΔCt method using *UBE2D2* as an internal control. (**d**) Numbers below blots indicate relative band intensities as determined by ImageJ software. (**e**) Specific binding of Hes1 to the *BNIP3* promoter. HPEK cells were infected with adenoviral constructs expressing hemagglutinin (HA)-tagged Hes1, and processed for chromatin immunoprecipitation (ChIP) with an anti-HA antibody and normal rabbit immunoglobulin G (Cont rab-IgG) as a nonimmune control. Q-PCR amplification of the region of the *BNIP3* gene described in the indicated map (upper panel; nucleotides −360 to −244 (1); nucleotides −247 to −87 (2); −212 to +22 (3)) was also performed. The amount of precipitated DNA was calculated relative to the total input chromatin. All the data represent the average of three independent experiments ± SD. $^{**}P<0.01$.

with a BNIP3 adenoviral vector. BNIP3 expression was found to be sufficient to trigger the formation of EGFP-LC3 puncta that was significantly reduced by addition of 3-methyladenine (3-MA), an inhibitor of autophagy (Figure 3a and b). On the other hand, BNIP3 knockdown markedly decreased the punctuate distribution of EGFP-LC3 in differentiated HPEKs (Figure 3c and d). Furthermore, flow cytometry analysis using a green fluorescent probe used to specifically detect autophagy (Cyto-ID autophagy detection dye) (Chan *et al.*, 2012) also showed that BNIP3 was required for the autophagy induction (Figure 3c and f). These data indicate that BNIP3 is involved in the induction of autophagy in HPEKs. Intriguingly, these data also confirm the previous finding that autophagosome induction is accompanied by keratinocyte differentiation (Haruna *et al.*, 2008). We observed that the number of mitochondria was decreased in the granular layers, where BNIP3 expression and autophagosome formation was observed (Figure 4a). In addition, mitochondria were significantly decreased in the differentiated HPEKs *in vitro* (Figure 4b). Colocalizations of mitochondria and EGFP-LC3 dot were observed only in the differentiating keratinocytes (Figure 4c), suggesting the contribution of autophagy in the decrease of mitochondria. BNIP3 expression was also correlated with decreased mitochondria in HPEKs, whereas addition of 3-MA restored mitochondrial numbers (Figure 4d). Furthermore, we also observed colocalization of mitochondria and EGFP-LC3 dot in BNIP3-overexpressing HPEKs (Figure 4e). These data indicated that mitochondria were removed by BNIP3-induced autophagy. Next, we investigated the involvement of BNIP3 in the differentiation of epidermal keratinocytes. Western blot analysis and immunofluorescent staining revealed that BNIP3 expression increased during differentiation (Figure 5a and b). Knockdown of BNIP3 significantly suppressed keratinocyte differentiation when the cells were treated with differentiation medium (Figure 5c and d), indicating that BNIP3 is required for terminal differentiation of keratinocyte. On the other hand, forced expression of BNIP3 in HPEKs markedly stimulated loricrin expression (Figure 5e and f). To determine whether BNIP3-dependent keratinocyte differentiation was induced by autophagy, 3-MA was added to the cells transduced with BNIP3. As shown in Figure 5e and f, 3-MA notably abolished the keratinocyte differentiation induced by BNIP3, suggesting that BNIP3 is required for terminal differentiation of keratinocyte by induction of autophagy.

BNIP3 maintains epidermal keratinocytes

To further determine the roles of BNIP3 in epidermal differentiation, the human skin epidermal equivalent was reconstituted from HPEKs stably expressing a BNIP3 RNA interference (RNAi). Unfortunately, we did not observe drastic differentiation defects; however, we unexpectedly discovered

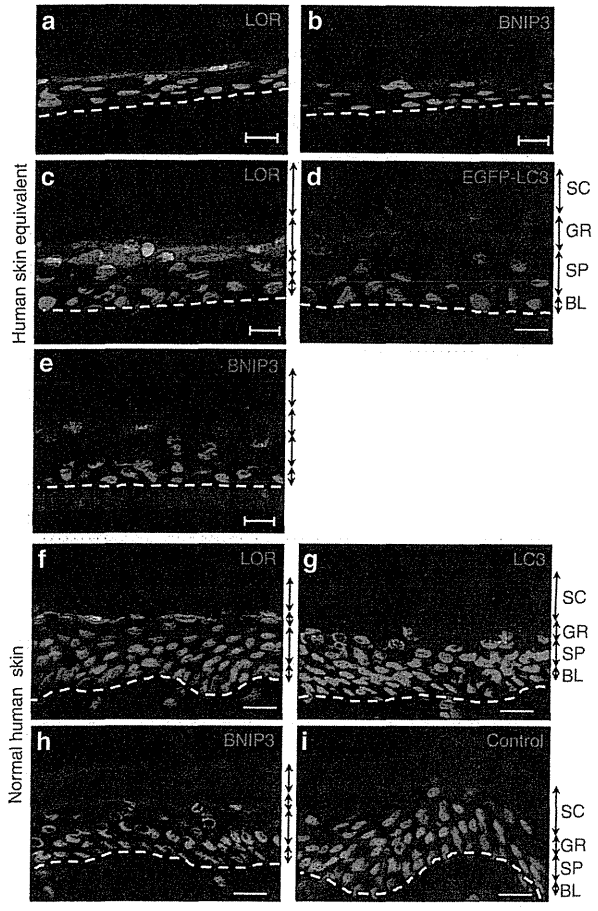

Figure 2. BNIP3 (BCL2 and adenovirus E1B 19-kDa-interacting protein 3) is expressed in the granular layer of the human epidermis. (**a–e**) Human skin epidermal equivalents were constituted from (**a–d**) normal human primary epidermal keratinocytes (HPEKs) or (**e**) HPEKs transfected with EGFP-LC3 by lentiviral vector. Cells were grown for (**a**, **b**) 18 days and (**c–e**) 24 days after exposure at the air–liquid interface. (**f–i**) Normal human skin epidermis. (**a**, **c**, **f**) Expression pattern of loricrin (LOR). (**b**, **e**, **h**) Expression pattern of BNIP3. (**i**) Control staining without BNIP3 antibody is shown. (**d**) Autophagosome formation determined by EGFP-LC3 puncta. (**g**) Endogenous expression pattern of LC3. The blue signals indicate nuclear staining. The dotted lines indicate (**a–e**) the boundary between the epidermis and the membrane or (**f–i**) the boundary between the epidermis and the dermis. Scale bars = 20 μm. BL, basal layer; GL, granular layer; SC, stratum corneum (cornified layer); SP, spinous layer.

that "sunburn-like cells" existed in BNIP3 knockdown epidermal equivalent (Figure 6a and b). We therefore hypothesized that BNIP3 might play a key role in the survival of epidermal keratinocytes. To evaluate this hypothesis, HPEKs were irradiated with 20 mJ cm^{-2} UVB. UVB irradiation triggered the formation of autophagosome that was significantly reduced by BNIP3 knockdown (Figure 6c–e). As shown in Figure 6f, UVB irradiation induced cleavage of caspase3 and BNIP3 expression. Intriguingly, knockdown of UVB-induced BNIP3 by RNAi further increased the amount of cleaved caspase3, suggesting that BNIP3 is required for the protection of keratinocytes from UVB-induced apoptosis (Figure 6f).

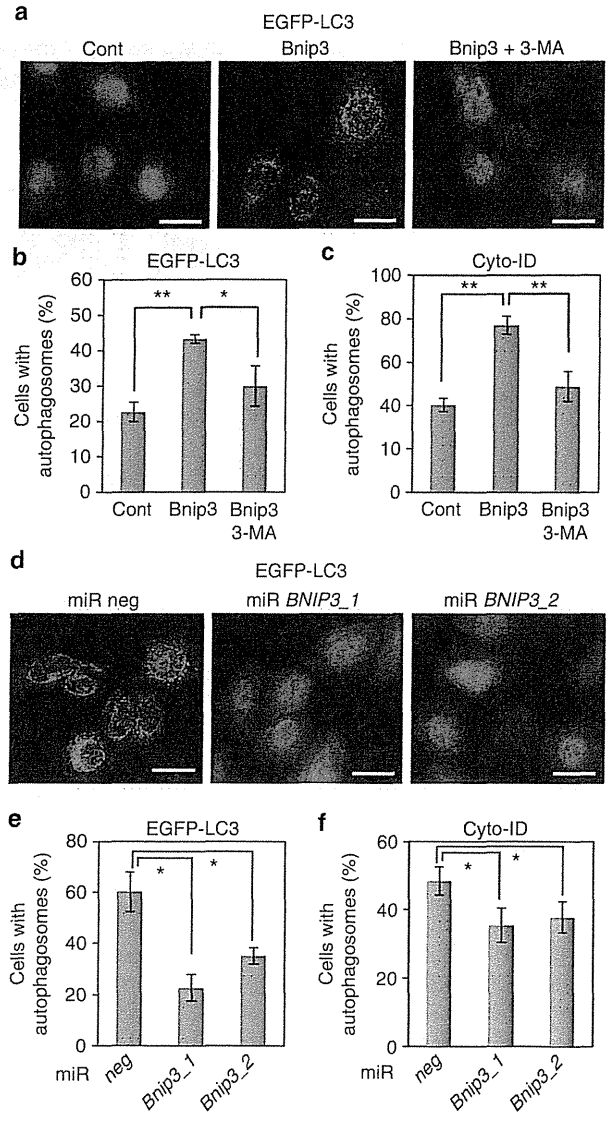

Figure 3. BNIP3 (BCL2 and adenovirus E1B 19-kDa-interacting protein 3) stimulates autophagy. (**a**, **b**) EGFP-LC3-expressing human primary epidermal keratinocytes (HPEKs) were transduced with DsRed (Cont) or BNIP3. As an inhibitor of autophagy, 3-methyladenine 3-MA (5 mM) was added. Cells were then stained with anti-EGFP at 24 hours after transduction. (**a**) EGFP-LC3 staining is shown in green. Scale bars = 20 μm. (**b**) The percentage of EGFP-LC3-positive cells with more than five puncta were quantified and are presented as the mean of three independent experiments ± SD. (**c**) HPEKs were transduced with DsRed (Cont) or BNIP3. As an inhibitor of autophagy, 3-MA (5 mM) was added. Autophagy induction was determined by Cyto-ID staining and quantified by flow cytometry. (**d**, **e**) EGFP-LC3-expressing HPEKs were transduced with miR *neg*, miR *BNIP3_1*, or miR *BNIP3_2* and induced to differentiate. Cells were then stained with anti-EGFP at 8 hours after differentiation induction. (**d**) EGFP-LC3 staining is shown in green. Scale bars = 20 μm. (**e**) The percentage of EGFP-LC3-positive cells with more than five puncta were quantified and are presented as the mean of three independent experiments ± SD. (**f**) HPEKs were transduced with miR *neg*, miR *BNIP3_1*, or miR *BNIP3_2* and induced to differentiate. Autophagy induction was determined by Cyto-ID staining and quantified by flow cytometry. All the data represent the average of three independent experiments ± SD. $^{**}P < 0.01$; $^{*}0.01 < P < 0.05$.

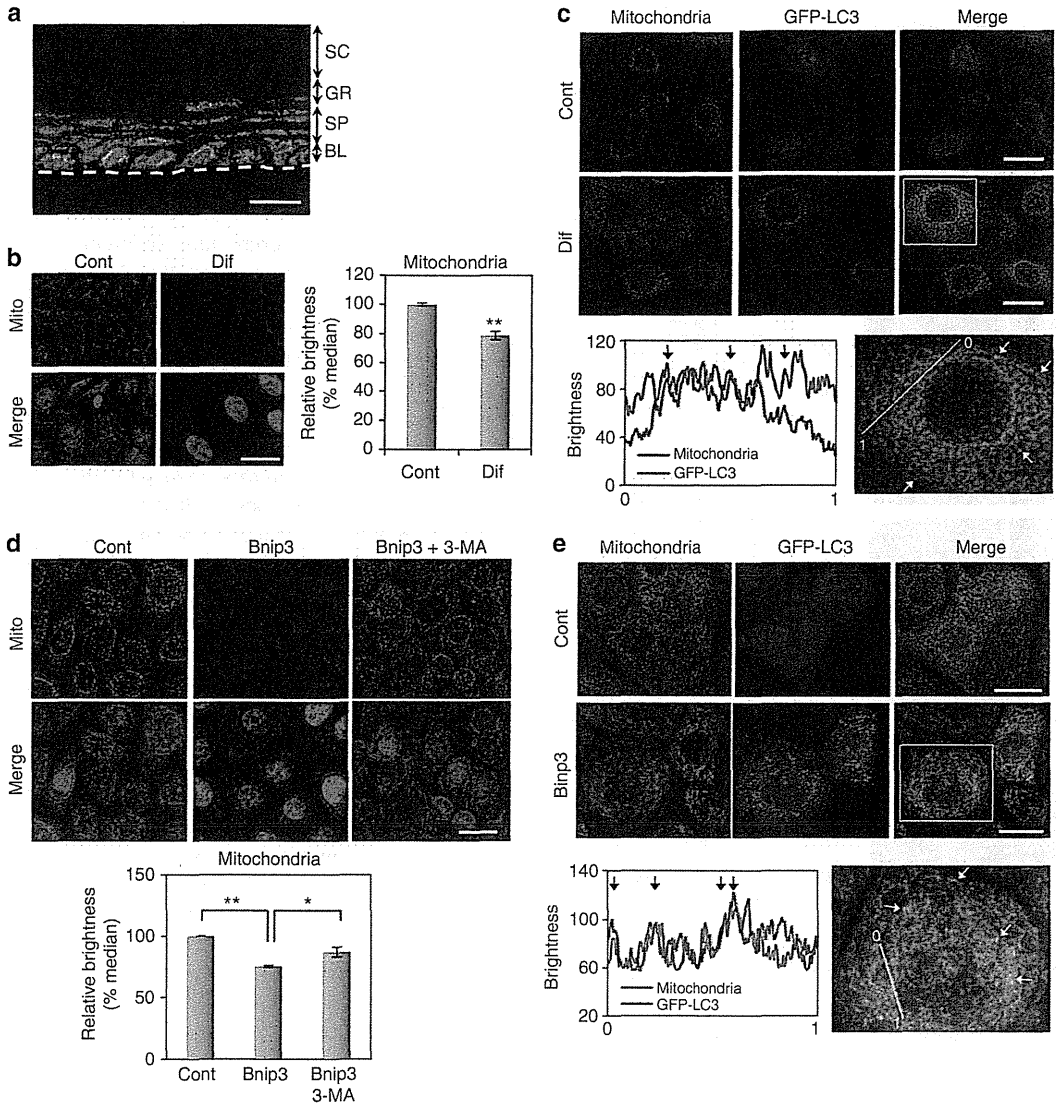

Figure 4. Autophagy stimulates mitochondrial degradation. (**a**) Distribution pattern of mitochondria. The blue signals indicate nuclear staining. The dotted lines indicate the boundary between the epidermis and the membrane. Scale bars = 20 μm. BL, basal layer; GL, granular layer; SC, stratum corneum (cornified layer); SP, spinous layer. (**b**) Nondifferentiated control (Cont) or differentiated human primary epidermal keratinocytes (HPEKs; Dif) were subjected to immunofluorescent staining 2 days after induction of differentiation. Mitochondrial staining is shown in red. The blue signals indicate nuclear staining. Scale bar = 20 μm. The graph indicates the percent of median brightness calculated by BZ Analyzer Software (Keyence) as the mean of three independent experiments ± SD. (**c**) EGFP-LC3-expressing HPEKs were differentiated. Cont or Dif were stained with anti-mitochondria (red) and anti-EGFP (green) 8 hours after induction of differentiation. Graph indicates the linescan analysis of the red and green fluorescent channels. Initial point of linescan is indicated as 0, and terminal point is indicated as 1. The arrows mark the colocalization of the two proteins. (**d**) HPEKs were transduced with enhanced green fluorescent protein (EGFP; Cont) or BNIP3 (BCL2 and adenovirus E1B 19-kDa-interacting protein 3). As an inhibitor of autophagy, 3-methyladenine 3-MA (5 mM) was added. Cells were then fixed and stained with anti-mitochondria 48 hours after transduction. Scale bar = 20 μm. The graph indicates the percent of median brightness calculated by BZ Analyzer Software (Keyence) as the mean of three independent experiments. $^{**}P<0.01$; $^{*}0.01<P<0.05$. (**e**) EGFP-LC3-expressing HPEKs were transduced with mock (Cont) or BNIP3. Cells were then fixed and stained with anti-mitochondria (red) and anti-EGFP (green) 24 hours after transduction. Graph indicates the linescan analysis of the red and green fluorescent channels. Initial point of linescan is indicated as 0, and terminal point is indicated as 1. The arrows mark the colocalization of the two proteins.

DISCUSSION

In this study, we demonstrated that BNIP3, a potent inducer of autophagy, plays a role in the terminal differentiation and maintenance of epidermal keratinocytes. It has been suggested that autophagy plays a role in the skin epidermis, but few attempts have been made to clarify the involvement of autophagy in skin epidermis.

We found that the HES1 transcriptional repressor directly suppressed BNIP3 expression in mouse epidermis and HPEKs (Figure 1). Moreover, our results revealed that BNIP3 was

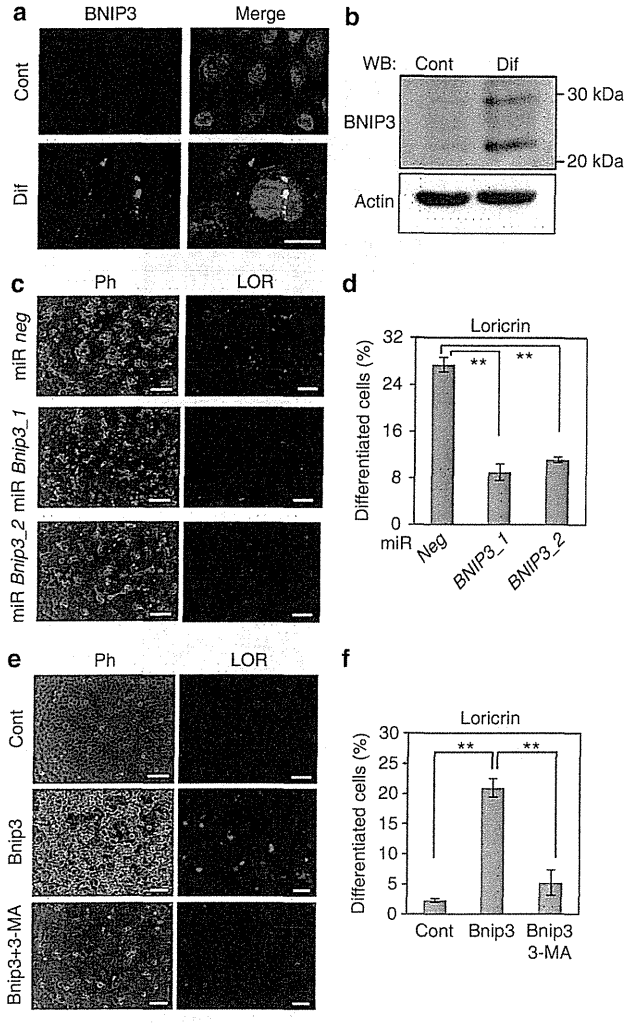

Figure 5. *BNIP3* (*BCL2* and adenovirus *E1B* 19-kDa-interacting protein 3) is required for the differentiation of keratinocytes *in vitro*. (**a**, **b**) Human primary epidermal keratinocytes (HPEKs) were differentiated and BNIP3 expression was observed. (**a**) Nondifferentiated control (Cont) or differentiated HPEKs (Dif) were subjected to immunofluorescent staining. BNIP3 staining is shown in green. Mitochondrial staining is shown in red. The blue signals indicate nuclear staining. Scale bar = 20 μm. (**b**) Western blot (WB) analysis. Proteins extracted from Cont or Dif were probed with anti-BNIP3 or anti-actin. (**c**, **d**) HPEKs were infected with adenoviral vectors expressing miR *neg*, miR *BNIP3_1*, or miR *BNIP3_2* followed by induction of differentiation. Cells were then immunostained with a loricrin antibody 9 days after transduction. (**e**, **f**) HPEKs were infected with adenoviral vectors expressing enhanced green fluorescent protein (EGFP; Cont) or BNIP3 and subjected to immunofluorescent staining against loricrin (LOR) 6 days after transduction. As an inhibitor of autophagy, 3-methyladenine 3-MA (5 mM) was added. Phase contrast images (Ph) and LOR staining are shown. Scale bars = 200 μm. (**d**, **f**) Percentages of LOR-positive differentiated cells were calculated by computerized image analysis. The data represent the average of three independent experiments ± SD. $^{**}P < 0.01$.

expressed in the granular layers of mouse epidermis, its human skin epidermal equivalent, and its normal human skin epidermis (Figures 1 and 2). These data are consistent with our previous report showing that Hes1 is expressed in the spinous layers, where it represses the regulatory genes for differentiation to maintain the spinous cell fate (Moriyama *et al.*, 2008). Hence, it can be inferred that Bnip3 expression is suppressed in the spinous layers by Hes1, whereas it is upregulated in the granular layers where Hes1 expression is absent. In addition, our finding that BNIP3 is required for keratinocyte differentiation fits our idea that Hes1 represses certain regulatory genes to prevent the premature differentiation of spinous cells. Our *in vitro* data suggest that BNIP3 is involved in keratinocyte differentiation through autophagy (Figures 3–5). The mechanisms underlying the involvement of autophagy in keratinocyte differentiation remain elusive; however, considering that keratinocyte differentiation induced mitochondrial clearance and BNIP3 expression (Figure 4 and 5), BNIP3-induced autophagy may be responsible for the removal of mitochondria that may be required for the terminal differentiation of epidermal keratinocytes. During reticulocyte differentiation, programmed clearance of mitochondria induced by BNIP3L/Nix, a molecule closely related to BNIP3, has been reported to be a critical step (Schweers *et al.*, 2007). Therefore, keratinocytes likely possess the same differentiation mechanism that reticulocytes have, although further investigation will be required for elucidation.

In contrast to the results from differentiation in two-dimensional culture, we did not observe drastic differentiation defects in the BNIP3 knockdown human epidermal equivalent except for the existence of "sunburn-like cells" (Figure 6). This might be because of the incomplete suppression of BNIP3 in the BNIP3 knockdown keratinocytes, and/or might be because of the redundancy between BNIP3 and BNIP3L/Nix, a homolog of BNIP3, as we found in our preliminary study that Bnip3l is also expressed in the epidermis (data not shown). Although the phenotypes of BNIP3-null mice were published in 2007, these researchers found that BNIP3-null mice had no increase in mortality or apparent physical abnormalities (Diwan *et al.*, 2007). Generally, impairment of epidermal differentiation or skin barrier formation results in an obvious defect. Thus, BNIP3-null epidermis seems to exhibit subtle, if any, abnormalities. On the basis of these findings, the involvement of BNIP3 in epidermal differentiation must be investigated in the future. In-depth analysis of the BNIP3-null epidermis phenotype could help elucidate the role of BNIP3 in mouse epidermal differentiation.

Despite the lack of obvious differentiation defects in the human epidermal equivalent, our data showing that BNIP3 knockdown caused the appearance of "sunburn-like cells" is regarded as an example of apoptosis (Young, 1987), revealing a new role of BNIP3 in keratinocyte maintenance. Furthermore, requirement of BNIP3 for protection from UV-induced apoptosis was confirmed in two-dimensional keratinocyte cultures (Figure 6e). The underlying mechanism of this prosurvival function of BNIP3 in keratinocytes remains unclear; however, previous reports have demonstrated that hypoxia-induced autophagy through BNIP3 is critical for the prosurvival process (Bellot *et al.*, 2009). Recently, it has been reported that UVA induces autophagy to remove oxidized phospholipids and protein aggregates in epidermal keratino-

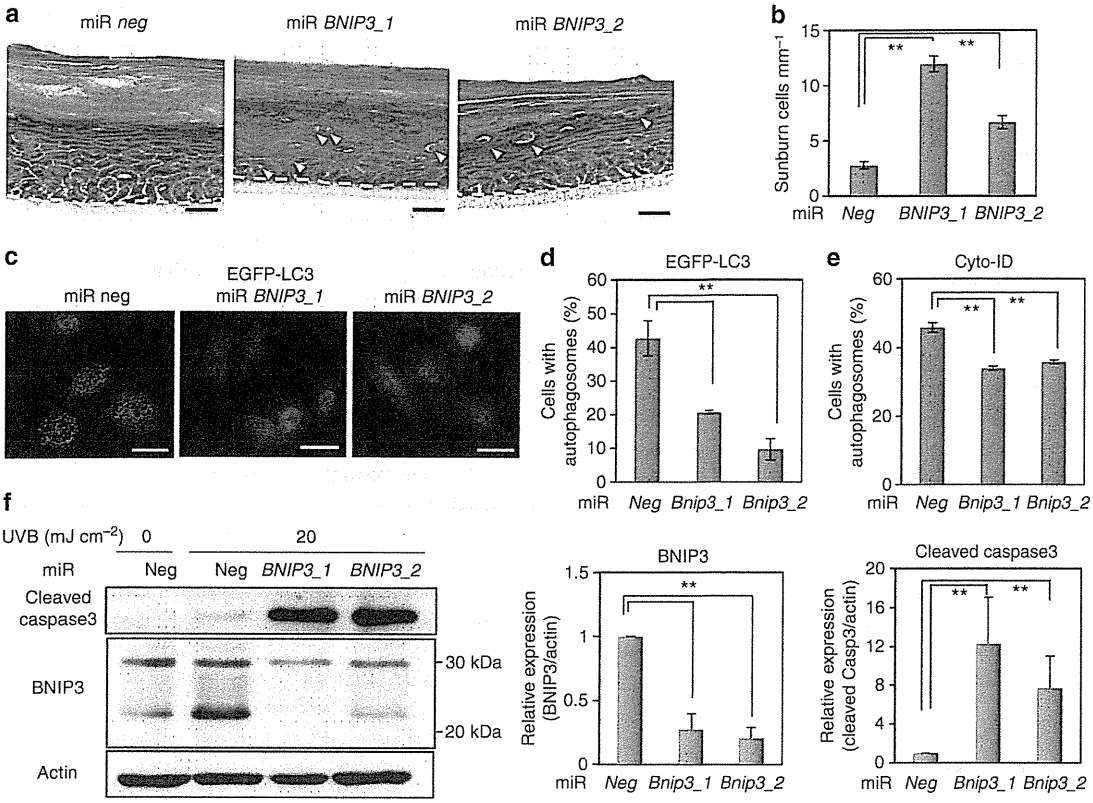

Figure 6. BNIP3 (BCL2 and adenovirus E1B 19-kDa-interacting protein 3) promotes cell survival in the reconstituted epidermis and keratinocytes. (**a**) Morphology of the human skin epidermal equivalents from human primary epidermal keratinocytes (HPEKs) infected with lentivirus expressing miR *neg*, miR *BNIP3_1*, or miR *BNIP3_2*. Arrowheads indicate sunburn-like cells. (**b**) The number of sunburn-like cells per mm was counted and plotted as the means of 10 sections ± SD. (**c–e**) HPEKs were infected with adenovirus expressing miR *neg*, miR *BNIP3_1*, or miR *BNIP3_2*, and irradiated with UVB. (**c**) Cells were stained with anti-EGFP at 8 hours after UVB irradiation. (**d**) The percentage of EGFP-LC3-positive cells with more than five puncta were quantified and are presented as the mean of three independent experiments ± SD. (**e**) Autophagy induction was determined by Cyto-ID staining and quantified by flow cytometry. The data represent the average of three independent experiments ± SD. (**f**) Cells were subjected to western blot analysis at 8 hours after irradiation. The blot shown is representative image of three independent experiments. Graphs indicate relative band intensities as determined by ImageJ software and plotted as the means of three independent experiments. Scale bars = 20 μm. $^{**}P<0.01$.

cytes (Zhao *et al.*, 2013). Because our data indicate that UVB-induced autophagy is mediated by BNIP3 (Figure 6c and d), it is possible that autophagy induced by BNIP3 also plays a role in the maintenance of keratinocytes. Further analysis is required to confirm these results.

UV-induced apoptotic cells appear within 12 hours and are predominately located in the suprabasal differentiated keratinocyte compartment of human skin (Gilchrest *et al.*, 1981). Moreover, differentiated keratinocytes appear to be most sensitive to the UV light that induces p53-dependent apoptosis (Tron *et al.*, 1998). Tron *et al.* (1998) demonstrated that differentiated keratinocytes in p53-null mice exhibited only a small increase in apoptosis after UVB irradiation compared with the increase observed in normal control animals (Tron *et al.*, 1998). Interestingly, because p53 has been reported to directly suppress BNIP3 expression (Feng *et al.*, 2011), BNIP3 might be abundantly upregulated in suprabasal cells in p53-null animals, resulting in the resistance to UVB-induced apoptosis. Indeed, our preliminary study showed that p53 knockdown enhanced UV-induced BNIP3 expression in HPEKs (data not shown). Therefore, BNIP3 expression in suprabasal cells appears to be important for the protection of differentiated keratinocytes from normal environmental stress such as weak UV exposure *in vivo*.

A recent report on a role for autophagy in epidermal barrier formation and function was identified in *atg7*-deficient mice (Rossiter *et al.*, 2013). The authors showed that autophagy was constitutively active in the suprabasal epidermal layers as we report in this study (Figure 2). However, in contradiction to our results, the authors concluded that autophagy was not essential for the barrier function of the skin. This may be because of the presence of an alternative Atg5/Atg7-independent autophagic pathway (Nishida *et al.*, 2009) in the epidermis. This Atg5/Atg7-independent pathway is also independent of LC3, but forms Rab9-positive double-membrane vesicles. Moreover, protein degradation via this pathway is inhibited by 3-MA and is dependent on Beclin 1. Our data demonstrate that: (1) BNIP3 induced the formation of

EGFP-LC3 puncta (Figure 4) and (2) 3-MA significantly diminished the formation of GFP-LC3 puncta and keratinocyte differentiation induced by BNIP3 (Figure 5). These findings suggest that BNIP3 in the epidermis induced both conventional and Atg5/Atg7-independent autophagy. Intriguingly, GFP cleaved from GFP-LC3 also accumulates in the *Atg7*-deficient epidermis (Rossiter *et al.*, 2013), thereby demonstrating the existence of an alternative autophagic pathway (Juenemann and Reits, 2012) in the epidermis. Further investigation will be required to determine whether Beclin 1 and Rab9 are indispensable for the BNIP3-induced autophagy and subsequent differentiation of keratinocytes.

In summary, our data reveal that expression of BNIP3 in granular cells induces autophagy and is involved in the terminal differentiation and maintenance of skin epidermis. Studies on the involvement of autophagy in skin epidermis have attracted considerable attention recently. In addition, increasing evidence suggests the involvement of BNIP3 in the differentiation of several cell types, including oligodendrocytes (Itoh *et al.*, 2003), osteoclasts (Knowles and Athanasou, 2008), and chondrocytes (Zhao *et al.*, 2012); however, the precise role of BNIP3 in this process remains to be investigated. Our study thus provides new insights into the functions of BNIP3 in differentiation and homeostasis.

MATERIALS AND METHODS

Histology and immunofluorescent analysis

Samples and embryos were fixed in 4% paraformaldehyde, embedded in optimal cutting temperature compound, frozen, and sectioned at 10 μm. Sections were then either subjected to hematoxylin and eosin staining or immunohistochemical analysis as previously described (Moriyama *et al.*, 2006). Details are described in Supplementary Materials Online.

Cell culture

HPEKs were purchased from CELLnTEC (Bern, Switzerland) and maintained in CnT-57 (CELLnTEC) culture medium according to the manufacturer's protocol. For induction of differentiation, the medium was changed to CnT-02 (CELLnTEC) at confluent monolayers of HPEKs, followed by adding calcium ions to 1.8 mM. The generation of human skin equivalents was performed using CnT-02-3DP culture medium (CELLnTEC) according to the manufacturer's protocol.

Design of artificial microRNAs and plasmid construction

Oligonucleotides targeting a human BNIP3 sequence compatible for use in cloning into BLOCK-iT Pol II miR RNAi expression vectors (Invitrogen, Carlsbad, CA) were obtained using the online tool BLOCK-iT RNAi Designer. The oligonucleotide sequences used in this study are shown in Supplementary Table S1 online. Cloning procedures were performed following the manufacturer's instructions.

Adenovirus and lentivirus infection

Adenoviruses expressing EGFP, Hes1, BNIP3, and miR *BNIP3* were constructed using the ViraPower adenoviral expression system (Invitrogen) according to the manufacturer's protocol. Lentivirus expressing EGFP-LC3 (from Addgene plasmid 21073, Cambridge, MA) and miR *BNIP3* plasmid was constructed and used to infect keratinocytes as previously described (Moriyama *et al.*, 2012; Moriyama *et al.*, 2013).

RNA extraction, complementary DNA generation, and Q-PCR

Total RNA extraction, complementary DNA generation, and Q-PCR analyses were carried out as previously described (Moriyama *et al.*, 2012). Details of the primers used in these experiments are shown in Supplementary Table S2 online.

Western blot analysis

Western blot analysis was performed as previously described (Moriyama *et al.*, 2012; Moriyama *et al.*, 2013). Details are described in Supplementary Materials Online.

ChIP assay

The ChIP assay was performed using the SimpleChIP Enzymatic Chromatin IP Kit (Magnetic Beads) (Cell Signaling Technology, Danvers, MA) according to the manufacturer's instructions. Hemagglutinin-tagged Hes1 was immunoprecipitated with rabbit polyclonal antibody against hemagglutinin tag (ab9110, Abcam, Cambridge, MA). Immunoprecipitated DNA was analyzed by Q-PCR. Relative quantification using a standard curve method was performed, and the occupancy level for a specific fragment was defined as the ratio of immunoprecipitated DNA over input DNA. Details of the primers used in these experiments are shown in Supplementary Table S2 online.

Flow cytometry analysis

For autophagy detection, Cyto-ID Autophagy detection kit (Enzo Life Sciences, Plymouth Meeting, PA) was used according to the manufacturer's instructions. Details are described in Supplementary Materials Online.

CONFLICT OF INTEREST

The authors state no conflict of interest.

ACKNOWLEDGMENTS

We thank Shogo Nomura, Ayumi Kitagawa, and Riho Ishihama for technical support; Dr Takashi Ueno for helpful discussions; Dr Hiroyuki Miyoshi for the CSII-EF-RfA, pCMV-VSVG-RSV-Rev, and pCAG-HIVg/p plasmids; Dr Tamotsu Yoshimori for pEGFP-LC3 plasmid; and Dr Ryoichiro Kageyama for *Hes1* KO mice. This work was supported by MEXT KAKENHI grant 23791304 to MM. This work was also supported in part by grants from the Ministry of Health, Labor, and Welfare of Japan and a grant from the Program for Promotion of Fundamental Studies in Health Sciences of the National Institute of Biomedical Innovation (NIBIO).

SUPPLEMENTARY MATERIAL

Supplementary material is linked to the online version of the paper at http://www.nature.com/jid

REFERENCES

Aymard E, Barruche V, Naves T *et al.* (2011) Autophagy in human keratinocytes: an early step of the differentiation? *Exp Dermatol* 20:263–8

Bellot G, Garcia-Medina R, Gounon P *et al.* (2009) Hypoxia-induced autophagy is mediated through hypoxia-inducible factor induction of BNIP3 and BNIP3L via their BH3 domains. *Mol Cell Biol* 29:2570–81

Blanpain C, Lowry WE, Pasolli HA *et al.* (2006) Canonical notch signaling functions as a commitment switch in the epidermal lineage. *Genes Dev* 20:3022–35

Chan LL, Shen D, Wilkinson AR *et al.* (2012) A novel image-based cytometry method for autophagy detection in living cells. *Autophagy* 8:1371–82

Chatterjea SM, Resing KA, Old W *et al.* (2011) Optimization of filaggrin expression and processing in cultured rat keratinocytes. *J Dermatol Sci* 61:51–9

Diwan A, Krenz M, Syed FM *et al.* (2007) Inhibition of ischemic cardiomyocyte apoptosis through targeted ablation of Bnip3 restrains postinfarction remodeling in mice. *J Clin Invest* 117:2825–33

Feng X, Liu X, Zhang W *et al.* (2011) p53 directly suppresses BNIP3 expression to protect against hypoxia-induced cell death. *EMBO J* 30: 3397–415

Gilchrest BA, Soter NA, Stoff JS *et al.* (1981) The human sunburn reaction: histologic and biochemical studies. *J Am Acad Dermatol* 5:411–22

Hamacher-Brady A, Brady NR, Logue SE *et al.* (2007) Response to myocardial ischemia/reperfusion injury involves Bnip3 and autophagy. *Cell Death Differ* 14:146–57

Haruna K, Suga Y, Muramatsu S *et al.* (2008) Differentiation-specific expression and localization of an autophagosomal marker protein (LC3) in human epidermal keratinocytes. *J Dermatol Sci* 52:213–5

Ishibashi M, Moriyoshi K, Sasai Y *et al.* (1994) Persistent expression of helix-loop-helix factor HES-1 prevents mammalian neural differentiation in the central nervous system. *EMBO J* 13:1799–805

Itoh T, Itoh A, Pleasure D (2003) Bcl-2-related protein family gene expression during oligodendroglial differentiation. *J Neurochem* 85:1500–12

Juenemann K, Reits EA (2012) Alternative macroautophagic pathways. *Int J Cell Biol* 2012:189794

Kabeya Y, Mizushima N, Ueno T *et al.* (2000) LC3, a mammalian homologue of yeast Apg8p, is localized in autophagosome membranes after processing. *EMBO J* 19:5720–8

Knowles HJ, Athanasou NA (2008) Hypoxia-inducible factor is expressed in giant cell tumour of bone and mediates paracrine effects of hypoxia on monocyte-osteoclast differentiation via induction of VEGF. *J Pathol* 215:56–66

Lippens S, Denecker G, Ovaere P *et al.* (2005) Death penalty for keratinocytes: apoptosis versus cornification. *Cell Death Differ* 12(Suppl 2):1497–508

Mellor HR, Rouschop KM, Wigfield SM *et al.* (2010) Synchronised phosphorylation of BNIP3, Bcl-2 and Bcl-xL in response to microtubule-active drugs is JNK-independent and requires a mitotic kinase. *Biochem Pharmacol* 79:1562–72

Mizushima N, Levine B (2010) Autophagy in mammalian development and differentiation. *Nat Cell Biol* 12:823–30

Mizushima N, Yamamoto A, Matsui M *et al.* (2004) In vivo analysis of autophagy in response to nutrient starvation using transgenic mice expressing a fluorescent autophagosome marker. *Mol Biol Cell* 15:1101–11

Mizushima N, Yoshimori T, Levine B (2010) Methods in mammalian autophagy research. *Cell* 140:313–26

Moriyama H, Moriyama M, Sawaragi K *et al.* (2013) Tightly regulated and homogeneous transgene expression in human adipose-derived mesenchymal stem cells by lentivirus with tet-off system. *PLoS One* 8:e66274

Moriyama M, Durham AD, Moriyama H *et al.* (2008) Multiple roles of Notch signaling in the regulation of epidermal development. *Dev Cell* 14:594–604

Moriyama M, Moriyama H, Ueda A *et al.* (2012) Human adipose tissue-derived multilineage progenitor cells exposed to oxidative stress induce neurite outgrowth in PC12 cells through p38 MAPK signaling. *BMC Cell Biol* 13:21

Moriyama M, Osawa M, Mak SS *et al.* (2006) Notch signaling via Hes1 transcription factor maintains survival of melanoblasts and melanocyte stem cells. *J Cell Biol* 173:333–9

Nishida Y, Arakawa S, Fujitani K *et al.* (2009) Discovery of Atg5/Atg7-independent alternative macroautophagy. *Nature* 461:654–8

Ohtsuka T, Ishibashi M, Gradwohl G *et al.* (1999) Hes1 and Hes5 as notch effectors in mammalian neuronal differentiation. *EMBO J* 18:2196–207

Quinsay MN, Thomas RL, Lee Y *et al.* (2010) Bnip3-mediated mitochondrial autophagy is independent of the mitochondrial permeability transition pore. *Autophagy* 6:855–62

Rossiter H, Konig U, Barresi C *et al.* (2013) Epidermal keratinocytes form a functional skin barrier in the absence of Atg7 dependent autophagy. *J Dermatol Science* 71:67–75

Sassone J, Colciago C, Marchi P *et al.* (2010) Mutant Huntingtin induces activation of the Bcl-2/adenovirus E1B 19-kDa interacting protein (BNip3). *Cell Death Dis* 1:e7

Schweers RL, Zhang J, Randall MS *et al.* (2007) NIX is required for programmed mitochondrial clearance during reticulocyte maturation. *Proc Natl Acad Sci USA* 104:19500–5

Sowter HM, Ratcliffe PJ, Watson P *et al.* (2001) HIF-1-dependent regulation of hypoxic induction of the cell death factors BNIP3 and NIX in human tumors. *Cancer Res* 61:6669–73

Srinivas V, Bohensky J, Shapiro IM (2009) Autophagy: a new phase in the maturation of growth plate chondrocytes is regulated by HIF, mTOR and AMP kinase. *Cells Tissues Organs* 189:88–92

Tron VA, Trotter MJ, Tang L *et al.* (1998) p53-regulated apoptosis is differentiation dependent in ultraviolet B-irradiated mouse keratinocytes. *Am J Pathol* 153:579–85

Vengellur A, LaPres JJ (2004) The role of hypoxia inducible factor 1alpha in cobalt chloride induced cell death in mouse embryonic fibroblasts. *Toxicol Sci* 82:638–46

Walls KC, Ghosh AP, Ballestas ME *et al.* (2009) bcl-2/Adenovirus E1B 19-kd interacting protein 3 (BNIP3) regulates hypoxia-induced neural precursor cell death. *J Neuropathol Exp Neurol* 68:1326–38

Young AR (1987) The sunburn cell. *Photodermatology* 4:127–34

Zhang J, Ney PA (2009) Role of BNIP3 and NIX in cell death, autophagy, and mitophagy. *Cell Death Differ* 16:939–46

Zhao Y, Chen G, Zhang W *et al.* (2012) Autophagy regulates hypoxia-induced osteoclastogenesis through the HIF-1alpha/BNIP3 signaling pathway. *J Cell Physiol* 227:639–48

Zhao Y, Zhang CF, Rossiter H *et al.* (2013) Autophagy is induced by UVA and promotes removal of oxidized phospholipids and protein aggregates in epidermal keratinocytes. *J Invest Dermatol* 133:1629–37

Stem Cell Reports
Resource
OPEN ACCESS

Long-Term Self-Renewal of Human ES/iPS-Derived Hepatoblast-like Cells on Human Laminin 111-Coated Dishes

Kazuo Takayama,[1,2,3] Yasuhito Nagamoto,[1,2] Natsumi Mimura,[2] Katsuhisa Tashiro,[4] Fuminori Sakurai,[1] Masashi Tachibana,[1] Takao Hayakawa,[5] Kenji Kawabata,[4] and Hiroyuki Mizuguchi[1,2,3,6,*]
[1]Laboratory of Biochemistry and Molecular Biology, Graduate School of Pharmaceutical Sciences, Osaka University, Osaka 565-0871, Japan
[2]Laboratory of Hepatocyte Differentiation, National Institute of Biomedical Innovation, Osaka 567-0085, Japan
[3]iPS Cell-Based Research Project on Hepatic Toxicity and Metabolism, Graduate School of Pharmaceutical Sciences, Osaka University, Osaka 565-0871, Japan
[4]Laboratory of Stem Cell Regulation, National Institute of Biomedical Innovation, Osaka 567-0085, Japan
[5]Pharmaceutical Research and Technology Institute, Kinki University, Osaka 577-8502, Japan
[6]The Center for Advanced Medical Engineering and Informatics, Osaka University, Osaka 565-0871, Japan
*Correspondence: mizuguch@phs.osaka-u.ac.jp
http://dx.doi.org/10.1016/j.stemcr.2013.08.006

SUMMARY

The establishment of self-renewing hepatoblast-like cells (HBCs) from human pluripotent stem cells (PSCs) would realize a stable supply of hepatocyte-like cells for medical applications. However, the functional characterization of human PSC-derived HBCs was not enough. To purify and expand human PSC-derived HBCs, human PSC-derived HBCs were cultured on dishes coated with various types of human recombinant laminins (LN). Human PSC-derived HBCs attached to human laminin-111 (LN111)-coated dish via integrin alpha 6 and beta 1 and were purified and expanded by culturing on the LN111-coated dish, but not by culturing on dishes coated with other laminin isoforms. By culturing on the LN111-coated dish, human PSC-derived HBCs were maintained for more than 3 months and had the ability to differentiate into both hepatocyte-like cells and cholangiocyte-like cells. These expandable human PSC-derived HBCs would be manageable tools for drug screening, experimental platforms to elucidate mechanisms of hepatoblasts, and cell sources for hepatic regenerative therapy.

INTRODUCTION

Human embryonic stem cells (hESCs) and human induced pluripotent stem cells (hiPSCs) have the ability to self-replicate and to differentiate into all types of body cells including hepatoblasts and hepatocytes. Although cryopreserved primary human hepatocytes are useful in drug screening and liver cell transplantation, they rapidly lose their functions (such as drug metabolism capacity) and hardly proliferate in in vitro culture systems. On the other hand, human hepatic stem cells from fetal and postnatal human liver are able to self-replicate and able to differentiate into hepatocytes (Schmelzer et al., 2007; Zhang et al., 2008). However, the source of human hepatic stem cells is limited, and these cells are not available commercially. Therefore, the human pluripotent stem cell (hPSC)-derived hepatoblast-like cells (HBCs), which have potential to differentiate into the hepatocyte-like cells, would be an attractive cell source to provide abundant hepatocyte-like cells for drug screening and liver cell transplantation.

Because expandable and multipotent hepatoblasts or hepatic stem cells are of value, suitable culture conditions for the maintenance of hepatoblasts or hepatic stem cells obtained from fetal or adult mouse liver were developed (Kamiya et al., 2009; Tanimizu et al., 2004). Soluble factors, such as hepatocyte growth factor (HGF) and epidermal growth factor (EGF), are known to support the proliferation of mouse hepatic stem cells and hepatoblast (Kamiya et al., 2009; Tanimizu et al., 2004). Extracellular matrix (ECM) also affects the maintenance of hepatoblasts or hepatic stem cells. Laminin can maintain the character of mouse hepatoblasts (Dlk1-positive cells) (Tanimizu et al., 2004). However, the methodology for maintaining HBCs differentiated from hPSCs has not been well investigated. Zhao et al. (2009) have reported that hESC-derived hepatoblast-like cells (sorted N-cadherin-positive cells were used) could be maintained on STO feeder cells. Although a culture system using STO feeder cells for the maintenance of hepatoblast-like cells might be useful, there are two problems. The first problem is that N-cadherin is not a specific marker for human hepatoblasts. N-cadherin is also expressed in hESC-derived mesendoderm cells and definitive endoderm (DE) cells (Sumi et al., 2008). The second problem is that residual undifferentiated cells could be maintained on STO feeder cells. Therefore, their culture condition cannot rule out the possibility of the proliferation of residual undifferentiated cells. Because it is known that hPSC-derived cells have the potential to form teratomas in the host, the production of safer hepatocyte-like cells or hepatoblast-like cells has been required. Therefore, we decided to purify hPSC-derived HBCs, which can differentiate into mature hepatocyte-like cells, and then expand these cells.

In this study, we attempt to determine a suitable culture condition for the extensive expansion of HBCs derived

from hPSCs. We found that the HBCs derived from hPSCs can be maintained and proliferated on human laminin-111 (LN111)-coated dishes. To demonstrate that expandable, multipotent, and safe (i.e., devoid of residual undifferentiated cells) hPSC-derived HBCs could be maintained under our culture condition, the hPSC-derived HBCs were used for hepatic and biliary differentiation, colony assay, and transplantation into immunodeficient mice.

RESULTS

Human PSC-Derived Hepatoblast-like Cells Could Adhere onto Human LN111 via Integrin α6 and β1

The HBCs were generated from hPSCs (hESCs and hiPSCs) as described in Figure 1A (details of the characterization of hPSC-derived HBCs are described in Figure 3). Definitive endoderm differentiation of hPSCs was promoted by stage-specific transient transduction of FOXA2 in addition to the treatment with appropriate soluble factors (such as Activin A). Overexpression of FOXA2 is not necessary for establishing the hPSC-derived HBCs, but it is helpful for efficient generation of the hPSC-derived HBCs. On day 9, these hESC-derived populations contained two cell populations with distinct morphology (Figure 1B). One population resembled human hepatic stem cells that were isolated from human fetal liver (shown in red) (Schmelzer et al., 2007), whereas the other population resembled definitive endoderm cells (shown in green) (Hay et al., 2008). The population that resembled human hepatic stem cells was alpha-1-fetoprotein (AFP) positive, whereas the other population was AFP negative (Figure 1C, left). On day 9, the percentage of AFP-positive cells was approximately 80% (Figure 1C, right). To characterize these two cell populations (hESC-derived HBC and non-HBC [NHBC] populations), the colonies were manually isolated by using a pipette, and then the gene expression analysis was performed. The gene expression levels of *AFP*, *CD133*, *EpCAM*, *CK8*, and *CK18* in the hESC-derived HBCs were higher than those in the bulk population containing both hESC-derived HBCs and NHBCs (*CD133*, *EpCAM*, *CK8*, and *CK18* were named as pan-hepatoblast markers and are known to be strongly expressed in both human hepatic stem cells and hepatoblasts [Schmelzer et al., 2007; Zhang et al., 2008]) (Figure 1D). On the other hand, the gene expressions of *AFP*, *CD133*, *EpCAM*, *CK8*, and *CK18* in the hESC-derived NHBCs were hardly detected. The gene expression levels of DE, mesendoderm, and pluripotent markers in the hESC-derived NHBCs were higher than those in the hESC-derived HBCs, indicating that the hESC-derived NHBCs could remain in a more undifferentiated state than the hESC-derived HBCs (Figures S1A–S1C available online). These results suggest that hepatoblast-like cells could be differentiated from hPSCs.

To purify the hESC-derived HBCs, these cells were plated onto dishes coated with various laminins. There are 15 different laminin isoforms in human tissues. Although laminin is known to be useful to sustain mouse hepatoblasts (Tanimizu et al., 2004), it remains unknown which human laminin isoform has the potential to purify and expand the HBCs. To identify a human laminin isoform that would be useful for purifying hESC-HBCs, the hESC-HBCs and -NHBCs were plated onto dishes coated with various types of commercially available human laminins (Figure 1E). The hESC-derived HBCs could more efficiently adhere onto the human LN111-coated dish compared with hESC-derived NHBCs or unseparated populations (containing both HBCs and NBCs). These data suggest that a hESC-derived HBC population can be purified from the unseparated populations by culturing on human LN111-coated dishes. Because integrins are known to be important molecules for cell adhesion to the ECM including laminins, we expected that certain types of integrins would allow selective adhesion of the hESC-derived HBCs to human LN111-coated dish. The gene expression levels of various integrins were examined (Figure 1F). Among the integrin α subunits, the gene expression level of *integrin α6* in the hESC-derived HBCs was significantly higher than that in the hESC-derived NHBCs. In contrast, among the integrin β subunits, the gene expression level of *integrin β1* was higher than those of *integrin β2* and *β3* in all cell populations. The hESC-derived HBCs, but not NHBCs, expressed both integrin α6 and β1 (Figure S1D). Almost all adhesion of the hESC-derived HBCs to a human LN111-coated dish was inhibited by both function-blocking antibodies to integrin α6 and β1 (Figure 1G). These results indicated that the hESC-derived HBCs could attach to a human LN111-coated dish via integrin α6 and β1.

The hPSC-Derived HBCs Could Be Proliferated and Maintained on a Human LN111-Coated Dish

To obtain the purified hESC-derived HBC population, the hESC-derived cells (day 9) were plated onto a human LN111-coated dish, and then unattached cells were removed at 15 min after plating (Figure 2A). Among various laminins, only human LN111 could proliferate (Figure 2B) and purify (Figure 2C) the AFP-positive population in the presence of HGF and EGF. During culture on the human LN111-coated dish, the morphology of the hESC-derived HBCs gradually changed into that of human hepatoblasts (Figure S1E) (Schmelzer et al., 2007). Therefore, the characteristics of hESC-derived HBCs might be changed by culturing on a human LN111-coated dish (details of the characterization of the hESC-derived HBCs are described in Figure 3). After culturing on a human LN111-coated

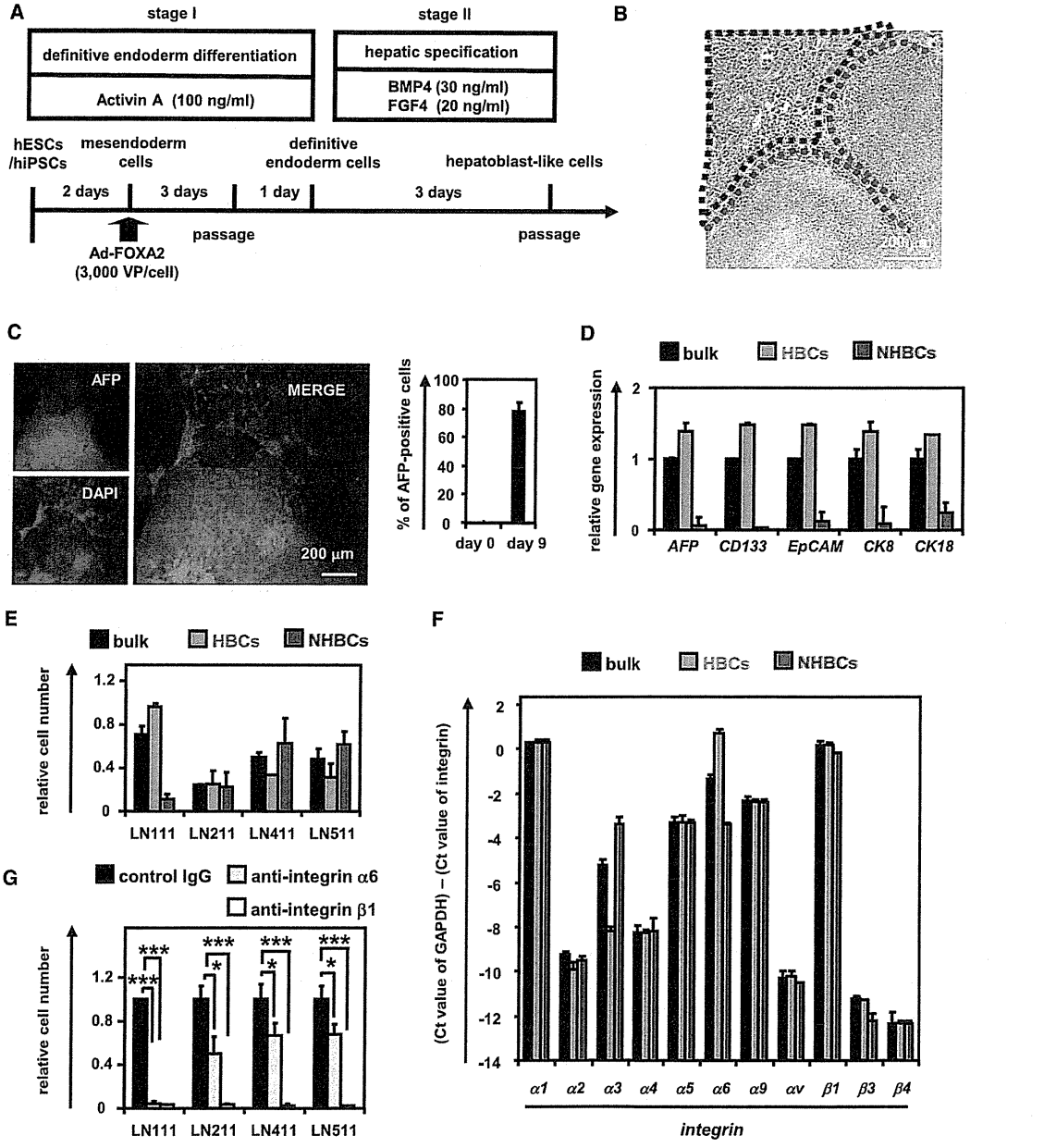

Figure 1. The Human ESC-Derived HBCs Selectively Attached to a Human LN111-Coated Dish via Integrin α6 and β1

(A) The procedure for the differentiation of hESCs (H9) into hepatoblast-like cells (HBCs) is presented schematically. Details are described in the Experimental Procedures.

(B) Phase-contrast micrographs of the hESC-derived HBCs (red) and non-HBCs (NHBCs) (green) are shown.

(C) The hESC-derived cells (day 9) were subjected to immunostaining with anti-AFP (red) antibodies. The percentage of AFP-positive cells was examined on day 0 or 9 by using FACS analysis. Data represent the mean ± SD from ten independent experiments. Cells on "day 0" and "day 9" were compared using Student's t test ($p < 0.01$).

(D) On day 9, the hESC-derived HBCs and NHBCs were manually picked, and the gene expression levels of *AFP* and pan-hepatoblast markers (*CD133*, *EpCAM*, *CK8*, and *CK18*) were measured by real-time RT-PCR. The gene expression levels of *AFP* and pan-hepatoblast markers in the hESC-derived cells (day 9; bulk) were taken as 1.0. Data represent the mean ± SD from four independent experiments. The gene expression levels in the HBCs were significantly different among the three groups (bulk, HBCs, and NHBCs) based on analysis with one-way ANOVA followed by Bonferroni post hoc tests ($p < 0.05$).

(legend continued on next page)